GCA-TR-67-5-N

PLANETARY METEOROLOGY

George Ohring Wen Tang Joseph Mariano

FINAL REPORT

Contract No. NASw-1227

March 1967

GCA CORPORATION
GCA TECHNOLOGY DIVISION
Bedford, Massachusetts

Prepared for

NATIONAL AERONAUTICS AND SPACE ADMINISTRATION
HEADQUARTERS
WASHINGTON 25, D. C.

FOREWORD

This final report is based upon research carried out during the past year under NASA contract NASw-1227, Planetary Meteorology. It contains complete discussions of two aspects of our research: 1) Seasonal and Latitudinal Variations of the Average Surface Temperature and Vertical Temperature Profile on Mars, and 2) The General Circulation of the Martian Atmosphere. A third task in our research, a review of available information on the meteorology of Mars and Venus, is discussed in a previously published technical report entitled Comprehensive Summary of Available Knowledge of the Meteorology of Mars and Venus by Edward M. Brooks (GCA Technical Report No. 66-21-N).

Abstracts for the two papers presented in this report may be found on the following pages; all references are listed together, starting on p. 61.

SEASONAL AND LATITUDINAL VARIATIONS OF THE AVERAGE SURFACE TEMPERATURE AND VERTICAL TEMPERATURE PROFILE ON MARS

George Ohring and Joseph Mariano

ABSTRACT

The seasonal and latitudinal variations of the average surface temperature and vertical profile of atmospheric temperature on Mars are computed using a thermal equilibrium model. In thermal equilibrium, the computed temperature profiles satisfy the following equilibrium conditions: 1) a balance at the top of the atmosphere between net incoming solar radiation and outgoing infrared radiation; 2) a balance at the surface between the net gain of heat by radiation and the loss of heat by convective transport into the atmosphere, the amount of convective loss being determined from the net integrated radiative cooling of the convective layer — the troposphere; and 3) the stratosphere is in radiative equilibrium. It is assumed that carbon dioxide is the sole radiating gas in a model atmosphere that is composed of 60 percent carbon dioxide and has a surface pressure of 10 mb. The results are presented in the form of pole-to-pole temperature cross-sections from the surface to about 40 km for each Martian season. Because the model does not allow for latitudinal transport of heat energy by the atmospheric circulation, the computed temperatures are too low at polar latitudes during the winter half of the year and probably too high at equatorial latitudes during the solstices and at polar latitudes during summer; they should be most representative of actual conditions at middle latitudes during the equinoxes and at low latitudes during the solstices. The computed temperature cross-sections indicate: 1) extremely small latitudinal temperature gradients in the summer hemisphere, with the maximum temperature occurring at the pole; 2) a decrease of tropopause altitude with latitude from a maximum at the equator during the equinoctial seasons and at the summer pole during the solstices; and 3) relatively isothermal vertical structure at high latitudes during the equinoxes and winter. Comparisons, where possible, of the present results with other theoretical studies and with the microwave and Mariner IV observational indications of Martian temperatures yield generally good agreement.

THE GENERAL CIRCULATION OF THE MARTIAN ATMOSPHERE

Wen Tang

ABSTRACT

Dynamic models simulating the Martian atmospheric circulation are constructed. Model I, based on a terrestrial atmospheric circulation model due to Adem (1962), is a vertically integrated model and is used to compute meridional profiles of mean mid-atmospheric zonal wind and temperature for both northern and southern hemispheres of Mars during the two equinoxes and the two solstices. In these experiments, the value of the eddy exchange coefficient is assumed to be 10^{10} cm^2 sec^{-1}, similar to that in the Earth's atmosphere. The numerical results indicate that the maximum mid-atmospheric wind is about 45 m sec^{-1} and occurs at about 40^{o} latitude in the winter hemisphere. The direction of the mean zonal wind for all seasons except summer is generally from the west. The mean mid-atmospheric temperatures during the solstices range from a maximum of $200^{o}K$ at the summer pole to $110^{o}K$ at the winter pole. During the equinoxes, the mean mid-atmospheric temperatures range from $175^{o}K$ to $195^{o}K$ at the equator to $140^{o}K$ to $142^{o}K$ at the poles.

Model II is a more sophisticated two-level, quasi-geostrophic numerical model. This model can be used to compute the latitudinal variation of surface temperature, zonal and meridional winds, and mid-atmospheric vertical velocities as a function of time during the course of a Martian year. The model is described in the text; application to Mars is planned during the coming year.

TABLE OF CONTENTS

LIST OF ILLUSTRATIONS

LIST OF ILLUSTRATIONS (Cont.)

1. SEASONAL AND LATITUDINAL VARIATIONS OF THE AVERAGE SURFACE TEMPERATURE AND VERTICAL TEMPERATURE PROFILE ON MARS

George Ohring and Joseph Mariano

1.1 Introduction

Previous theoretical estimates of the average vertical temperature profile in the lower Martian atmosphere have been based upon convective-radiative equilibrium models (see, for example, Goody, 1957; Prabhakara and Hogan, 1965; and Ohring and Mariano, 1966). In such models, a surface temperature is assumed and the vertical temperature profile is computed on the basis of a convective troposphere and radiative equilibrium stratosphere. In the present study, we actually compute the average surface temperature as well as the average vertical temperature profile as a function of latitude and season. The computations are based upon the thermal equilibrium concept of Manabe and Strickler (1964), which is a slight modification of the convective-radiative equilibrium model. Although the effect on Martian temperatures of latitudinal transport of heat by the atmospheric circulation is not included in the model, the computed temperatures should be useful for many purposes. Where possible, we compare the computed temperatures with observational and previous theoretical indications of Martian temperatures.

1.2 Basic Model

Under the concept of thermal equilibrium, the computed temperature profile must satisfy the following equilibrium conditions: 1) a balance at the top of the atmosphere between net incoming solar radiation and net outgoing infrared radiation; 2) a balance at the surface between the net gain of heat by radiation and the loss of heat by convective transport into the atmosphere; the loss of heat by convective transfer into the atmosphere is determined from the net integrated radiative cooling of the convective layer — the troposphere; and 3) the stratosphere is in radiative equilibrium.

The thermal equilibrium temperature profile is computed with the use of an iterative procedure based upon the initial value method of computing radiative equilibrium temperatures. Starting with an initial temperature profile, one computes the vertical distribution of the rate of radiational temperature change. These rates are applied to the initial profile for a unit time step to obtain a new temperature profile. This process is continued until the three equilibrium conditions are satisfied. At each stage of the calculations any layers with lapse rates greater than a specified convective lapse rate are corrected to the convective lapse rate. Numerically, this is accomplished as follows.

(1) In a non-convective layer, the net rate of temperature change at time step τ is equal to the computed rate of radiational temperature change:

$$\left(\frac{\partial\theta}{\partial t}\right)^{\tau}_{net} = \left(\frac{\partial\theta}{\partial t}\right)^{\tau}_{rad} \quad . \tag{1}$$

(2) In a convective layer (that is, a layer that would have a super-convective lapse rate if no correction were made) that does not extend to the surface, the net rate of temperature change must satisfy the following requirements:

$$\int_{p_t}^{p_b} \left(\frac{\partial\theta}{\partial t}\right)^{\tau}_{net} dp = \int_{p_t}^{p_b} \left(\frac{\partial\theta}{\partial t}\right)^{\tau}_{rad} dp \tag{2}$$

where p_t and p_b are the pressures at the top and base of the layer, respectively, and

$$\left(\frac{\partial\theta}{\partial p}\right)^{\tau+1} = \text{convective lapse rate} \tag{3}$$

where

$$\theta^{\tau+1} = \theta^{\tau} + \left(\frac{\partial\theta}{\partial t}\right)^{\tau}_{net} \Delta t \tag{4}$$

(3) In a convective layer that extends to the surface, the net rate of temperature change must satisfy (3) and (4) and

$$\frac{c_p}{g}\int_{p_t}^{p_o} \left(\frac{\partial\theta}{\partial t}\right)^{\tau}_{net} dp = \frac{c_p}{g}\int_{p_t}^{p_o} \left(\frac{\partial\theta}{\partial t}\right)^{\tau}_{rad} dp + S_g + (F\downarrow_g)^{\tau} - \left(\sigma\theta_g^{\,4}\right)^{\tau+1} \tag{5}$$

where c_p is the specific heat of the atmosphere at constant pressure, g is the gravitational acceleration, p_o is the surface pressure, S_g is the net downward flux of solar radiation at the surface, $(F\downarrow_g)^{\tau}$ is the downward flux of infrared radiation at the surface at time step τ, and $(\sigma\theta_g^{\,4})^{\tau+1}$ is the upward flux of radiation at the surface at time step $\tau+1$. This equation is a result of the second equilibrium condition; it enables us to compute the surface temperature at each succeeding time step. At each time step, Equations (1) through (5) must be satisfied before computations for the next time step begin.

1.3 Infrared Cooling

The radiative rates of temperature change depend upon two factors — infrared cooling and solar heating. Thus,

$$\left(\frac{\partial\theta}{\partial t}\right)_{rad} = \left(\frac{\partial\theta}{\partial t}\right)_{s} + \left(\frac{\partial\theta}{\partial t}\right)_{IR} . \tag{6}$$

In this section, we discuss the model used to compute infrared fluxes and cooling rates $(\partial\theta/\partial t)_{IR}$ in the Martian atmosphere. In the next section, we discuss the model to compute the solar heating rates, $(\partial\theta/\partial t)_{s}$.

We shall make use of the computational model discussed by Rodgers and Walshaw (1966). They take as vertical coordinate the unit z, where

$$z = -\ell n\ \varphi \tag{7}$$

and $\varphi = p/p_o$, where p_o is the surface pressure. Then $(\partial\theta/\partial t)_{IR}$ can be written as

$$\left(\frac{\partial\theta}{\partial t}\right)_{IR} = -\frac{g}{c_p}\ \frac{C}{p} \tag{8}$$

where g is the gravitational acceleration, c_p is specific heat at constant pressure, and C is the derivative with respect to z of the net flux of infrared radiation. At any level z, C for an absorption band can be written as

$$C(z) = B(Z)\ \frac{dT}{dz}\ (z,Z) - \int_{o}^{Z} \frac{dT}{dz}\ (z,z')\ \frac{dB}{dz'},\ (z')\ dz' \tag{9}$$

where B is the blackbody flux for the absorption band, Z is the highest level considered, and T is the transmission function for the absorption band. For the Martian atmosphere, we can assume that only the 15μ CO_2 band contributes to the infrared cooling. Local thermodynamic equilibrium is also assumed. Curtis and Goody (1956) have found this to be a good assumption for the 15μ CO_2 band in the Earth's atmosphere down to pressures as low as 3.4×10^{-2} mb.

For a band transmission model we assume the Goody random model, for which the transmission of Lorentz lines (the applicability of the Lorentz line shape for the Martian atmosphere is discussed in the Appendix) along a path at constant pressure can be written as

$$T = \exp\left[-\frac{1.66\ km}{\delta}\ \left(1 + \frac{1.66\ km}{\pi\alpha}\right)^{-\frac{1}{2}}\right] \tag{10}$$

where k is the mean line intensity, α is the half-width of the absorption lines, m is the amount of carbon dioxide in g cm^{-2}, δ is the mean line spacing, and the factor 1.66 is introduced as a multiple of m to approximate flux transmission. For an atmosphere with constant mass mixing ratio, w, of CO_2, m between any two levels z and z′ is given by

$$m = \frac{wp_o}{g} [\varphi(z) - \varphi(z')] . \tag{11}$$

Equation (10) is for a homogeneous path, i.e., constant pressure and temperature. In the actual atmosphere, both pressure and temperature vary along the path. Pressure affects the half-widths of the absorption lines while temperature affects both their half-widths and intensities. However, the effect of temperature is a second order effect compared to the effect of pressure and CO_2 amount on the transmission. The Lorentz half-width of an absorption line at pressure p and temperature θ can be written as

$$\alpha = \alpha_s \left(\frac{p}{p_s}\right) \left(\frac{\theta_s}{\theta}\right)^{\frac{1}{2}} = \alpha_s \frac{p_o \varphi}{p_s} \left(\frac{\theta_s}{\theta}\right)^{\frac{1}{2}} \tag{12}$$

where α_s is the half-width at standard pressure, p_s, and standard temperature, θ_s. Since the temperature variation with altitude is much smaller than the pressure variation, and since the temperature correction is proportional to the square root of temperature, we may approximate the temperature effect by assuming an appropriate isothermal atmosphere for Mars with a temperature equal to θ. For an isothermal atmosphere, the Curtis-Godson approximation for the mean half-width of an absorption line for an atmospheric path with varying pressure yields

$$\bar{\alpha} = \frac{\int \alpha \, dm}{\int dm} \tag{13}$$

or, upon substitution of (12),

$$\bar{\alpha} = \frac{\alpha_s \left(\frac{\theta_s}{\theta}\right)^{\frac{1}{2}} \left(\frac{p_o}{p_s}\right) \int \varphi \, dm}{\int dm} . \tag{14}$$

After integration, (14) can be reduced to

$$\bar{\alpha} = \frac{\alpha_s}{2}\left(\frac{\theta_s}{\theta}\right)^{\frac{1}{2}}\left(\frac{p_o}{p_s}\right)\left[\frac{\varphi(z)^2 - \varphi(z')^2}{\varphi(z) - \varphi(z')}\right] \quad . \tag{15}$$

The effect of temperature on the line intensities can be incorporated following Rodgers and Walshaw (1966). The mean absorber amount between any two levels is corrected by the formula

$$\bar{m} = \int \Phi(\theta)\ dm \tag{16}$$

where

$$\Phi(\theta) = \frac{\sum k_i(\theta)}{\sum k_i(\theta_s)}$$

in which k is the line intensity and the summation is over all lines contributing to the absorption interval. Rodgers and Walshaw present the following empirical equation for $\Phi(\theta)$.

$$\log_e \Phi(\theta) = a(\theta - 260) + b(\theta - 260)^2 \tag{17}$$

where $a = 3.49 \times 10^{-3}$ and $b = -1.28 \times 10^{-6}$ for the 15μ CO_2 band. If we again assume that we can use a constant temperature correction, $\Phi(\theta)$ can come out of the integral and (16) becomes

$$\bar{m} = \Phi(\theta)\int dm = \frac{\Phi(\theta) w\ p_o}{g}\left[\varphi(z) - \varphi(z')\right] . \tag{18}$$

$\bar{\alpha}$ and $\bar{m}$ can now be substituted into the expression for the transmittance, Equation (10). For the CO_2 content and pressures prevailing on Mars,

$$\frac{1.66\ k\ \bar{m}}{\pi\ \bar{\alpha}} \gg 1$$

and, hence, (10) can be written as

$$T = \exp\left[-\frac{(1.66\ \pi\ \bar{\alpha}\ k\ \bar{m})^{\frac{1}{2}}}{\delta}\right] , \tag{19}$$

which, upon substitution for $\bar{\alpha}$ and $\bar{m}$, becomes

$$T = \exp\left\{ - \left[\frac{1.66\ \pi\ k\ \alpha_s}{2\delta^2} \left(\frac{\theta_s}{\theta} \right)^{\frac{1}{2}} \frac{p_o^2}{p_s} \frac{\Phi(\theta) w}{g} \left(\varphi(z)^2 - \varphi(z')^2 \right) \right]^{\frac{1}{2}} \right\} \quad (20)$$

To compute the cooling rates, we require dT/dz.

Letting

$$F = \frac{1.66\ \pi\ k\ \alpha_s}{2\delta^2} \left(\frac{\theta_s}{\theta} \right)^{\frac{1}{2}} \frac{p_o^2}{p_s} \frac{\Phi(\theta) w}{g} \quad , \quad (21)$$

we obtain for the vertical derivative of the transmittance

$$\frac{dT}{dz} = \frac{F\ \varphi(z)^2}{[\varphi(z)^2 - \varphi(z')^2]^{\frac{1}{2}}} \exp\left\{ - \left[F \left(\varphi(z)^2 - \varphi(z')^2 \right)^{\frac{1}{2}} \right] \right\}. \quad (22)$$

For the 15μ CO_2 band, centered at 667 cm^{-1} and extending over 170 cm^{-1}, Rodgers and Walshaw (1966) obtained the parameters k, δ, and α_s by fitting detailed quantum-mechanical calculations of line positions and intensities to the random model for band transmission. We use their values for the evaluation of transmission: $\alpha_s = 0.07$ cm^{-1}; $k/\delta = 718.7$ g^{-1} cm^2; and $\pi\alpha_s/\delta = 0.448$. For the constant temperature correction, we assume $\theta = 200^{\circ}K$.

The downward flux of infrared radiation at the surface, $F\downarrow_g$, required for Equation (5), is given by

$$F\downarrow_g = - T(o,Z)\ B(Z) + B(o) + \int_o^Z T(o,z') \frac{dB}{dz}, (z')\ dz'. \quad (23)$$

The blackbody flux $B(\theta)$ is the integral of the Planck function at temperature θ over the spectral interval $n_1 = 582$ cm^{-1} to $n_2 = 752$ cm^{-1}. To a high approximation for this spectral region and Martian temperatures it can be computed from

$$B(\theta) = \frac{\pi\ c_1 \theta^4}{c_2^4} \left[\exp\left(- \frac{c_2 n}{\theta} \right) \right] \left[\frac{c_2^3 n^3}{\theta^3} + 3 \frac{c_2^2 n^2}{\theta^2} + 6 \frac{c_2 n}{\theta} + 6 \right] \Bigg|_{n=n_2}^{n=n_1} \quad (24)$$

where $c_1 = 1.191 \times 10^{-5}$ erg cm sec^{-1} $steradian^{-1}$ and $c_2 = 1.4389$ cm deg^{-1}.

1.4 Solar Heating

For the solar heating, we shall assume that only the near infrared bands of carbon dioxide contribute to heating. Although small amounts of water vapor are present in the Martian atmosphere, the contribution of this gas to the solar heating rate and to the final temperature distribution is negligible compared to carbon dioxide (see Ohring and Mariano, 1966). We shall follow the method of Houghton (1963), which is based upon the experimental absorption data of Howard, et al (1955), Burch, et al (1960), and Seeley and Houghton (1961).

For a given time of year and latitude, the average amount of solar energy absorbed from a pressure level p to the top of the atmosphere during a Martian day can be written as

$$E = \left(\sum_{\ell} I_{o\ell} \, \overline{\cos \psi} \; A_{\ell} \right) r \tag{25}$$

where $I_{o\ell}$ is the intensity of solar radiation per wavenumber n at the top of the atmosphere in the ℓ-th absorption band, $\overline{\cos \psi}$ is the average cosine of the solar zenith angle for the day, A_{ℓ} is the integrated absorption of the ℓ-th band for the atmospheric column extending from the top of the atmosphere to the pressure level p along a slant path parallel to the solar beam, r is the fraction of the day that the sun is shining, and the summation extends over the carbon dioxide absorption bands. The heating rate at a pressure level p can be determined from

$$\left(\frac{d\theta}{dt} \right)_s = \frac{g}{c_p} \, \overline{\cos \psi} \cdot r \sum_{\ell} I_{o\ell} \frac{dA_{\ell}}{dp} \, . \tag{26}$$

Houghton's (1963) expressions for the integrated absorption are:

$$\text{Weak bands} \quad (\bar{p}m < x_{\ell}) \qquad A_{\ell} = a_{\ell} (\bar{p}m)^{\frac{1}{2}} \tag{27}$$

$$\text{Strong bands} \quad (\bar{p}m > x_{\ell}) \qquad A_{\ell} = b_{\ell} + c_{\ell} \log_{10} (\bar{p}m) \tag{28}$$

where p is in mb, m is in atmo-cm of CO_2, and a_{ℓ}, b_{ℓ}, c_{ℓ}, and x_{ℓ} are the empirically determined constants for the ℓ-th band. For a path extending from the top of an atmosphere with a constant mixing ratio, w, to a level whose pressure is p_i

$$\bar{p} = \frac{\int p \, dm}{m} = \frac{p_i}{2} \tag{29}$$

and

$$m = \frac{10^3 w}{g \rho_c} \cdot \overline{\sec \psi} \cdot p_i \tag{30}$$

where ρ_c is the density of CO_2 at STP.

With these equations for mean pressure and path length, the integrated absorption in cm^{-1} down to the level p_i is

$$A_\ell(p_i) = \begin{cases} a_\ell \left(\frac{1}{2} \frac{10^3 w}{g \rho_c} \overline{\sec \psi} \right)^{\frac{1}{2}} p_i , & \bar{p}_i m < x_\ell \\ b_\ell + 2c_\ell (.435) \ell n_e (p_i) + c_\ell (.435) \ell n_e \left(\frac{1}{2} \frac{10^3 w}{g \rho_c} \overline{\sec \psi} \right) & \bar{p}_i m > x_\ell \end{cases} \tag{31}$$

Differentiating with respect to p, we have

$$\frac{dA_\ell}{dp_i} = \begin{cases} a_\ell \left(\frac{1}{2} \frac{10^3 w \overline{\sec \psi}}{g \rho_c} \right)^{\frac{1}{2}} & \bar{p} m < x_\ell \\ \frac{2c_\ell (.435)}{p_i} & \bar{p} m > x_\ell \end{cases} \tag{32}$$

The empirical constants for the near-infrared absorption bands, after Houghton (1963), are shown in Table 1 along with the values of I_o at Mars' mean distance from the sun.

For the solar radiation reaching the surface, S_g, we may write

$$S_g = (1 - A)(S_o \, r \, \overline{\cos \psi} - E_g) , \tag{33}$$

where S_o is the intensity of solar radiation at Mars' distance from the sun, A is the Martian planetary albedo, and E_g is the amount of solar energy absorbed in the atmosphere, which is given by

$$E_g = \left(\sum I_{o\ell} \, \overline{\cos \psi} \, A_{g\ell} \right) r , \tag{34}$$

where $A_{g\ell}$ is determined from (31).

Table 1

Constants for the near-infrared CO_2 bands.

Band (μ)	I_o erg cm^{-2} $sec^{-1}(cm^{-1})^{-1}$	a	b	c	x
2.0	18.3	0.23			
1.6	25.0	0.02	weak only		
1.4	27.2	0.02			
4.3	5.6	8.4	- 11	37	15.4
2.7	11.8	1.87	-136	65	910

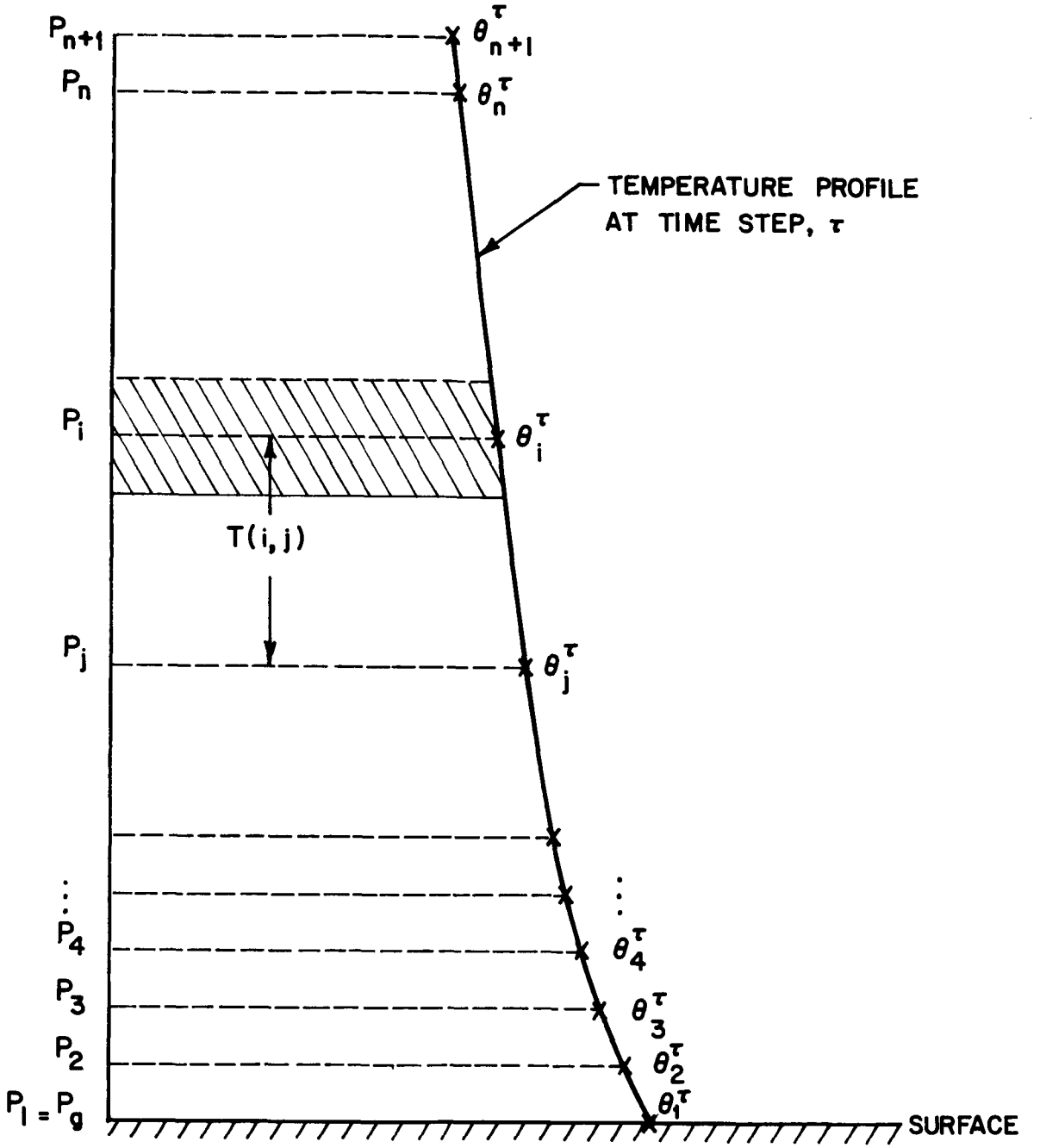

Figure 1. Schematic diagram of computational model at time step, τ.

Step (1): The infrared cooling rate is computed at each interface from

$$\left(\frac{d\theta}{dt}\right)_i^{\tau}IR = -\frac{g}{c_p}\frac{C(z_i)}{p_i}$$

$$= \frac{g}{c_p}\frac{1}{p_i}\left\langle -B(\theta_{n+1}^{\tau})\left(\frac{dT}{dz}\right)_{i,n+1}\right.$$

$$+\left\{\sum_{j=1}^{i-2}\frac{1}{2}\left[\left(\frac{dT}{dz}\right)_{i,j}+\left(\frac{dT}{dz}\right)_{i,j+1}\right]\cdot\left[B(\theta_{j+1}^{\tau})-B(\theta_j^{\tau})\right]\right.$$

$$+\left(\frac{dT}{dz}\right)_{i-\frac{1}{2}}\left[B(\theta_i^{\tau})-B(\theta_{i-1}^{\tau})\right]+\left(\frac{dT}{dz}\right)_{i+\frac{1}{2}}\left[B(\theta_{i+1}^{\tau})-B(\theta_i^{\tau})\right]$$

$$\left.\left.+\sum_{j=i+1}^{n}\frac{1}{2}\left[\left(\frac{dT}{dz}\right)_{i,j}+\left(\frac{dT}{dz}\right)_{i,j+1}\right]\cdot\left[B(\theta_{j+1}^{\tau})-B(\theta_j^{\tau})\right]\right\}\right\rangle \quad (40)$$

where $\left(\frac{dT}{dz}\right)_{i,j}$ is given by

$$\left(\frac{dT}{dz}\right)_{i,j} = \pm\frac{F^{\frac{1}{2}}\varphi_i^{\,2}}{[|\varphi_i^{\,2}-\varphi_j^{\,2}|]^{\frac{1}{2}}}\exp\left\{-\left[F(|\varphi_i^{\,2}-\varphi_j^{\,2}|)\right]^{\frac{1}{2}}\right\}\quad \begin{matrix} i<j \\ i>j \end{matrix} \quad (41)$$

where F is defined by (21).

Step (2): The solar heating rate is computed at each interface from

$$\left(\frac{\partial\theta}{\partial t}\right)_i S = \left(\sum_{\ell} I_{o\ell}\,\overline{\cos\psi}\,\frac{dA_\ell}{dp_i}\right) r \quad . \quad (42)$$

Step (3): The rate of change of temperature due to radiation is computed at each interface from

$$\left(\frac{\partial\theta}{\partial t}\right)_i^{\tau}rad = \left(\frac{\partial\theta}{\partial t}\right)_i S + \left(\frac{\partial\theta}{\partial t}\right)_i^{\tau}IR \quad (43)$$

Step (4): The loss of energy by the Martian surface due to convection is computed as follows. The convective temperature profile, $\{\theta_i^*\}$, with the surface temperature $\theta_g = \theta_i^\tau$, is computed for each successive level in the atmosphere from the equation

$$\frac{\theta_i^*}{\theta_{i-1}^*} = \left(\frac{p_i}{p_{i-1}} \right)^{\frac{\gamma-1}{\gamma}} \qquad (i = 2, 3, \ldots, \quad) \tag{44}$$

where $\gamma = c_p/c_v$, the ratio of the specific heat at constant pressure to the specific heat at constant volume, for the Martian atmosphere. The first computed convective temperature, θ_2^*, is compared with the new radiative temperature

$$(\theta_i)_{rad}^{\tau+1} = \theta_i^\tau + \left(\frac{\partial\theta}{\partial t} \right)_{i\,rad}^{\tau} \Delta t \ , \qquad (i = 2) \tag{45}$$

where Δt is the increment of time for the τ-th cycle. If $(\theta_2)_{rad}$ is superconvective, the net rate of change of temperature, $(\partial\theta/\partial t)_{net}$, is computed from the equation, (for i = 2)

$$\theta_i^* = \theta_i^\tau + \left(\frac{\partial\theta}{\partial t} \right)_{i\,net}^{\tau} \Delta t \ . \tag{46}$$

The above procedure is continued until the level where the new radiative temperature is not superconvective (say, i = t) is attained. This level (i = t) defines the top of the convective layer that extends to the surface. The new surface temperature, $\theta_g^{\tau+1}$, is now computed from (5) where

$$\int_{p_t}^{p_g} \left(\frac{\partial\theta}{\partial t} \right)_{net}^{\tau} dp \cong \sum_{i=2}^{t-1} \left(\frac{\partial\theta}{\partial t} \right)_{i\,net}^{\tau} \Delta p \tag{47}$$

$$\int_{p_t}^{p_g} \left(\frac{\partial\theta}{\partial t} \right)_{rad}^{\tau} dp \cong \sum_{i=2}^{t-1} \left(\frac{\partial\theta}{\partial t} \right)_{i\,rad}^{\tau} \Delta p \tag{48}$$

$$(F\downarrow_g)^\tau = \sum_{j=1}^{n} \frac{1}{2} \left[B(\theta_j^\tau) + B(\theta_{j+1}^\tau) \right] (T_{1j} - T_{1,j+1}) \tag{49}$$

(obtained from an integration by parts of (23)) and the solar radiation reaching the surface, S_g, is computed from (33). If the first new radiative temperature $(\theta_2)^{\tau+1}_{rad}$ is not superconvective, the model assumes that there is no convective layer that reaches the surface and (5) reduces to

$$0 = S_g + (F\downarrow_g)^{\tau} - (\sigma\theta_g^4)^{\tau+1} . \tag{50}$$

The new radiative temperatures $(\theta_i)^{\tau+1}_{rad}$ for $i > t$ are also compared to their corresponding convective values, θ^*_i. If one or more temperatures (say, from $i=\ell$ to $i=\ell+k$) are super convective, the net rates of change of temperature, $(\partial\theta/\partial t)^{\tau}_{i\,net}$ ($i = \ell, \ell+1, \ldots, \ell+k$) are computed from (46). Also, in order to satisfy Equation (2), the new radiative temperatures above the level, $\ell+k$, (say, from $\ell+k+1$ to $\ell+k+m$) are lowered to their corresponding convective values, where $(\partial\theta/\partial t)^{\tau}_{i\,net}$ ($i = \ell+k+1$ to $\ell+k+m$) is also computed from (46) and,

$$\sum_{i=\ell+1}^{\ell+k+m-1} \left[\left(\frac{\partial\theta}{\partial t} \right)^{\tau}_{i\,net} - \left(\frac{\partial\theta}{\partial t} \right)^{\tau}_{i\,rad} \right] \Delta p = 0 . \tag{51}$$

For the remaining new radiative temperatures that are not superconvective,

$$\left(\frac{\partial\theta}{\partial t} \right)^{\tau}_{i\,net} = \left(\frac{\partial\theta}{\partial t} \right)^{\tau}_{i\,rad} , \tag{52}$$

and thus Equation (1) is satisfied.

Step (5): The new temperature profile, $\{\theta_i^{\tau+1}\}$ is computed from the equations

$$\theta_i^{\tau+1} = \theta_i + \left(\frac{\partial\theta}{\partial t} \right)_{i\,net} \Delta t \qquad (i \geq 2, 3, \ldots, n) \tag{53}$$

and

$$\theta_1^{\tau+1} = \theta_g^{\tau+1} \tag{54}$$

and the τ-th interation cycle is completed. The iteration procedure is continued until the net rates of change of temperature, $(\partial\theta/\partial t)_{net}$ are less than a prescribed convergence criterion, ϵ.

1.6 Atmospheric Composition, Surface Pressure and Other Input Parameters

To perform the calculations with the thermal equilibrium model, information is required on the atmospheric composition and surface pressure on Mars. The results of recent spectroscopic observations (Spinrad et al, 1966; Owen, 1966; and Belton and Hunten, 1966) and the Mariner IV occultation experiment (Kliore et al, 1965) indicate that the surface pressure is about 5 to 10 mb and the atmosphere is predominantly carbon dioxide. For our computations, we assume an atmosphere composed of 60 percent (by mass) CO_2 with a surface pressure of 10 mb. The remainder of the atmosphere is probably argon or nitrogen — or a combination of the two — both of which are inactive as absorbers of radiation. We assume that the remaining gas is all nitrogen.

Trace amounts of water vapor — ~ 15μ precipitable cm — have been detected in the Martian atmosphere (Kaplan et al, 1964). However, previous calculations (Ohring and Mariano, 1966) suggest that inclusion of this gas in our model would not substantially change the results. Therefore, it is not included in the computations.

Several other input constants are required in the computations. The intensity of solar radiation at the top of the Martian atmosphere is taken as

$$S_o = \frac{s.c.}{R^2}$$

where s.c. = 2 cal cm^{-2} min^{-1} is the solar constant for Earth and R is the Mars-Sun distance in astronomical units. The variation of R with time of year is included in the calculations.

The planetary albedo of Mars is taken as 0.3 (de Vaucouleurs, 1964) and is assumed to be invariant with latitude and season. The convective lapse-rate is assumed to be the dry adiabatic lapse-rate. For the assumed atmospheric composition, the required thermodynamic constants are $(\gamma-1)/\gamma = 0.269$ and $c_p = 0.858 \times 10^7$ erg $gm^{-1}(^oK)^{-1}$. The iterations continued until the net rates of temperature change were less than the prescribed convergence criterion of $\epsilon = 0.05$ deg day^{-1}.

1.7 Results and Discussion

Before computing the average surface temperatures and atmospheric temperature profiles on Mars as a function of latitude and season, two preliminary sets of computations were performed. The first set was intended to compare results for an assumed model atmosphere (60% CO_2; p_o = 10 mb) with those for a 100 percent CO_2, p_o = 5 mb model atmosphere. The pure CO_2 atmosphere is also compatible with present observations and has been used in other calculations of Martian temperatures (see, for example, Leovy, 1966). The second set of computations was designed to determine the minimum number of layers in the computational model required to yield a reasonably accurate picture of the vertical temperature structure. Both sets of computations were performed for a time of maximum insolation - southern hemisphere summer solstice, latitude 80°S.

The results of the first set of computations are shown in Figure 2, where the computed temperatures are plotted as a function of p/p_o, the ratio of atmospheric pressure to surface pressure. The thermodynamic constants for the 5 mb, 100 percent CO_2 atmosphere are $(\gamma-1)/\gamma = 0.257$ and $c_p = 0.736 \times 10^7$ erg gm^{-1} $(°K)^{-1}$. The average surface temperature for the 10 mb case is slightly higher - 255°K versus 254°K - than for the 5 mb case. This is due to the slightly greater greenhouse effect (83 m STP of CO_2 at 10 mb pressure versus 69 m STP of CO_2 at 5 mb pressure) in the 10 mb atmospheric model. In addition, the greater adiabatic constant, $(\gamma-1)/\gamma$, for the 10 mb case also tends to increase the surface temperature, since the convective flux required to maintain an adiabatic temperature profile from the surface to the tropopause is less. The most significant feature of the computed temperature profiles, however, is the small temperature differences for the two different model atmospheres. The maximum temperature difference is 7°K and occurs at the upper levels. This result indicates that the temperatures computed with our assumed model atmosphere would also be representative of a 5 mb, 100 percent CO_2 model.

The results of the second set of computations are shown in Figure 3. In this set, a 10-layer computational model was compared to a 4-layer computational model. As can be seen, there is no appreciable difference in the computed temperature profiles. Therefore, the 4-layer model was used in computing the latitudinal distribution of temperature profiles for each of the four Martian seasons.

The computed temperature distributions are shown in Figures 4, 5, 6 and 7 in the form of latitudinal cross-sections - one for each season - extending from north pole to south pole. The vertical coordinate is the pressure plotted on a logarithmic scale; p = 1 mb corresponds to about 20 km altitude, p = 0.1 mb to about 40 km. Temperatures were computed at even 20-degree latitude intervals.

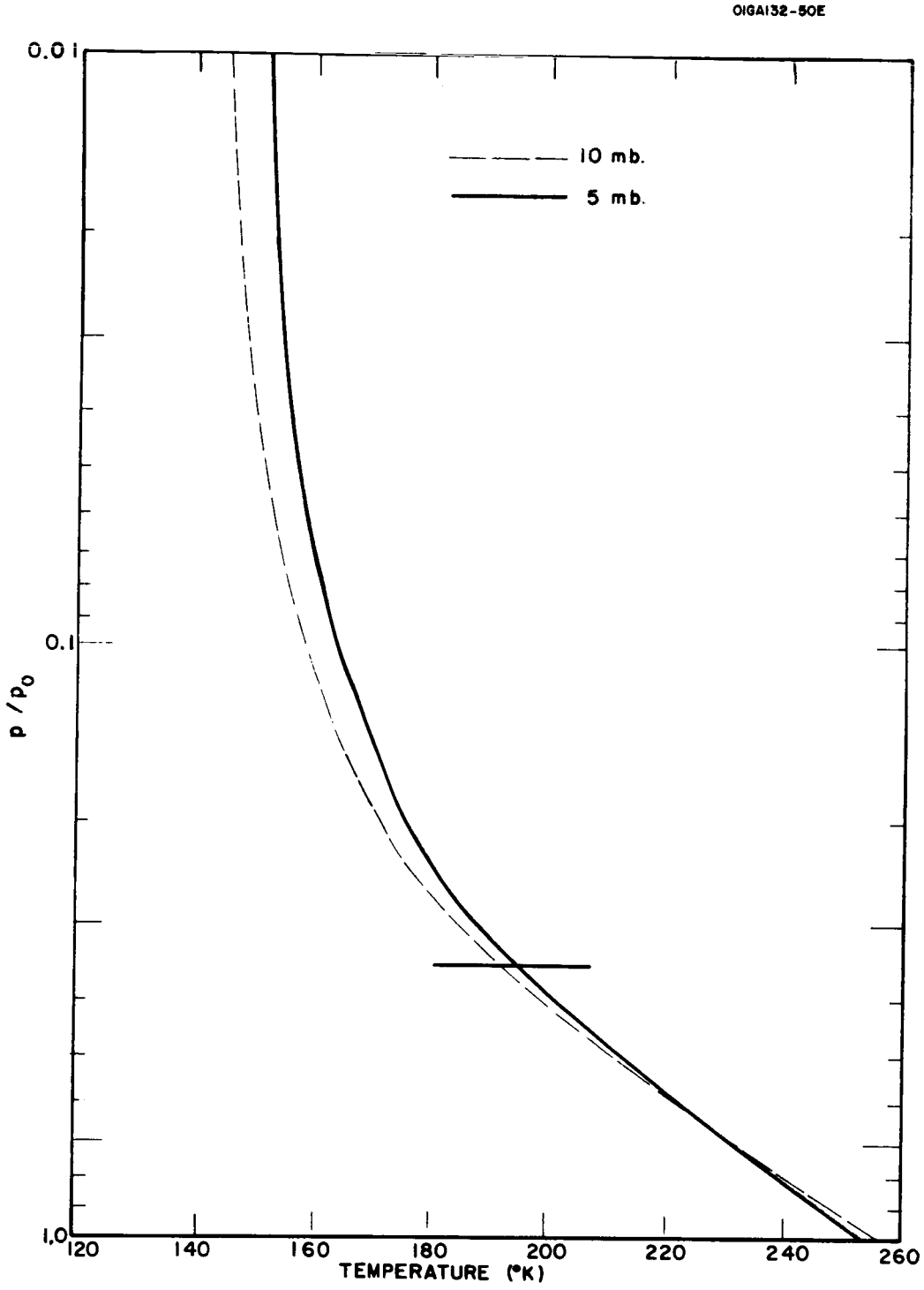

Figure 2. Comparison of Martian temperature profiles computed for 10 mb, 60% CO_2 atmosphere (dashed line) and 5 mb, 100% CO_2 atmosphere (solid line) for Southern Hemisphere summer solstice, latitude 80°S. Tropopause indicated by short horizontal line.

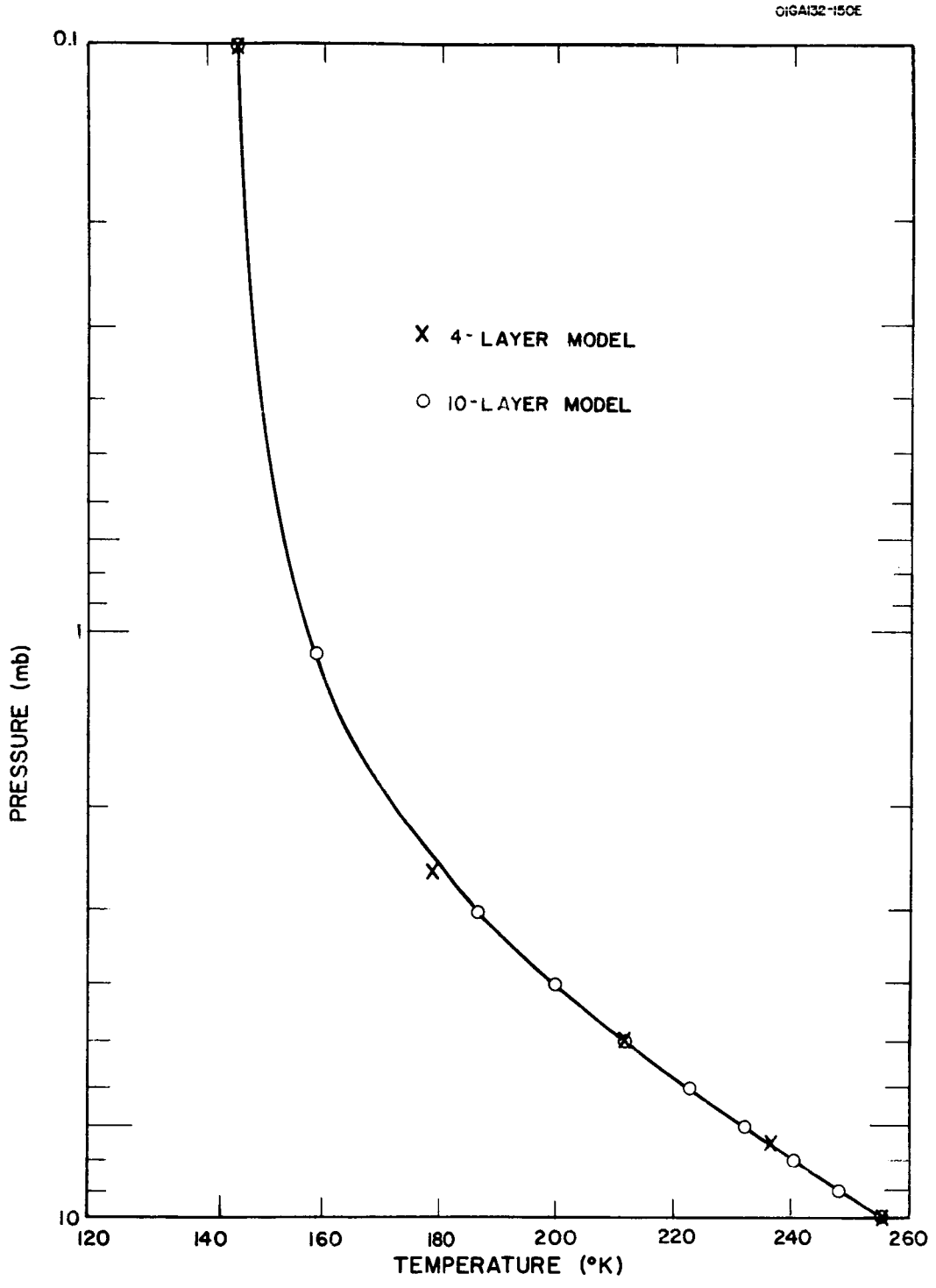

Figure 3. Comparison of Martian temperature profiles computed with 4-layer model (x) and 10-layer model (0) for Southern Hemisphere summer solstice, latitude 80°S.

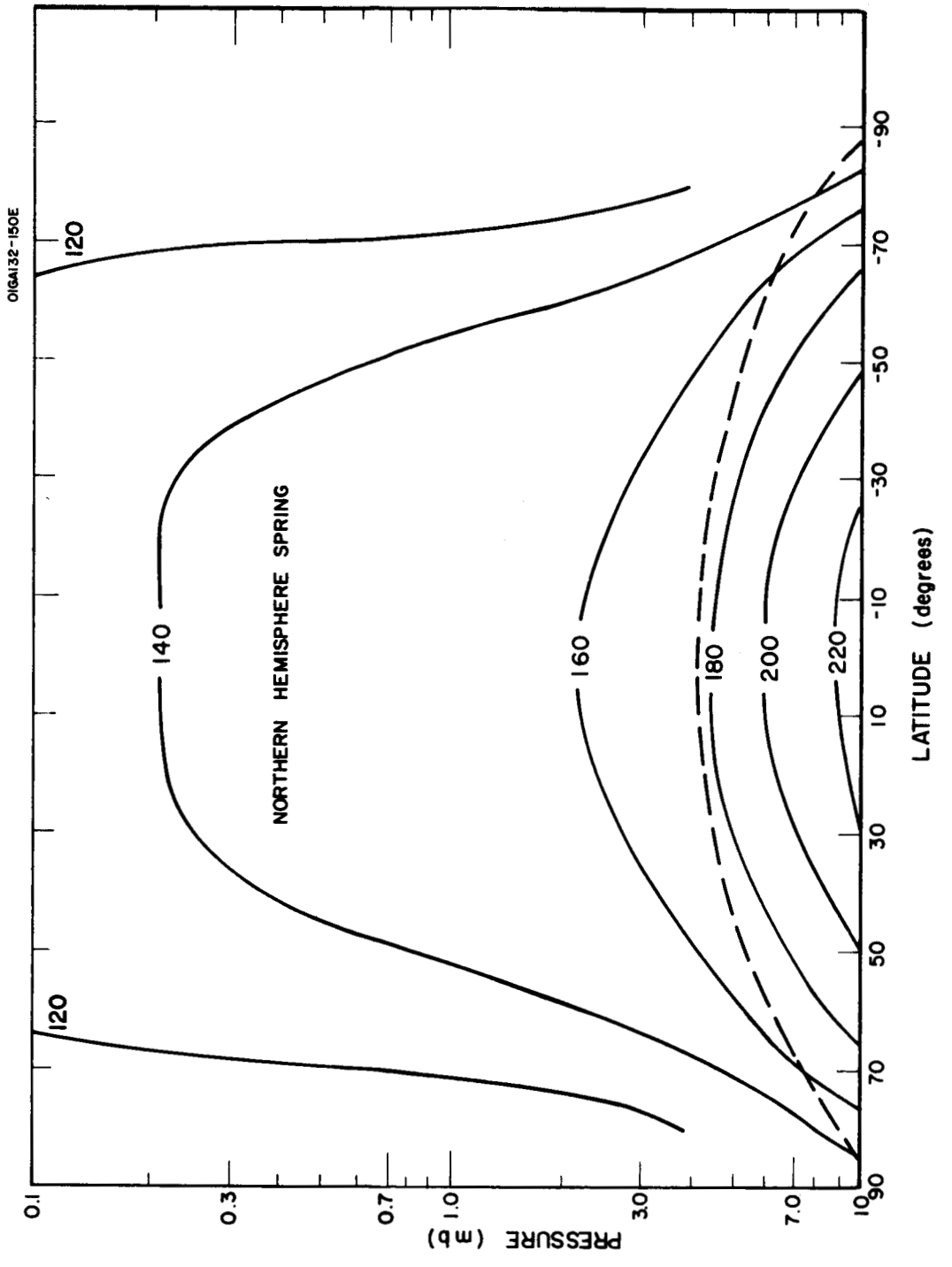

Figure 4. Computed latitudinal temperature cross-section for Northern Hemisphere spring equinox on Mars. Temperatures in ^{o}K; tropopause indicated by dashed line.

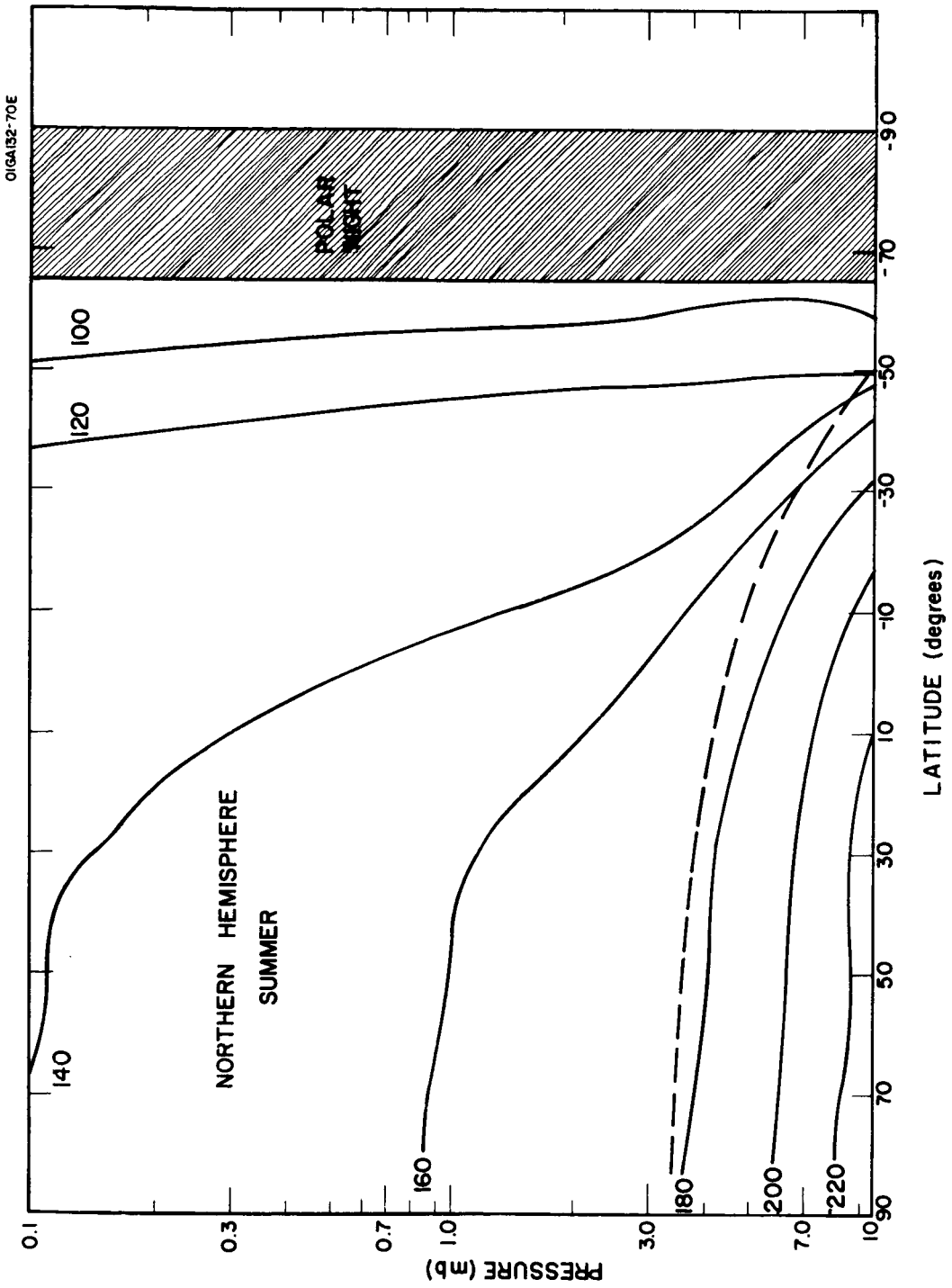

Figure 5. Computed latitudinal temperature cross-section for Northern Hemisphere summer solstice on Mars. Temperatures in ^{o}K; tropopause indicated by dashed line.

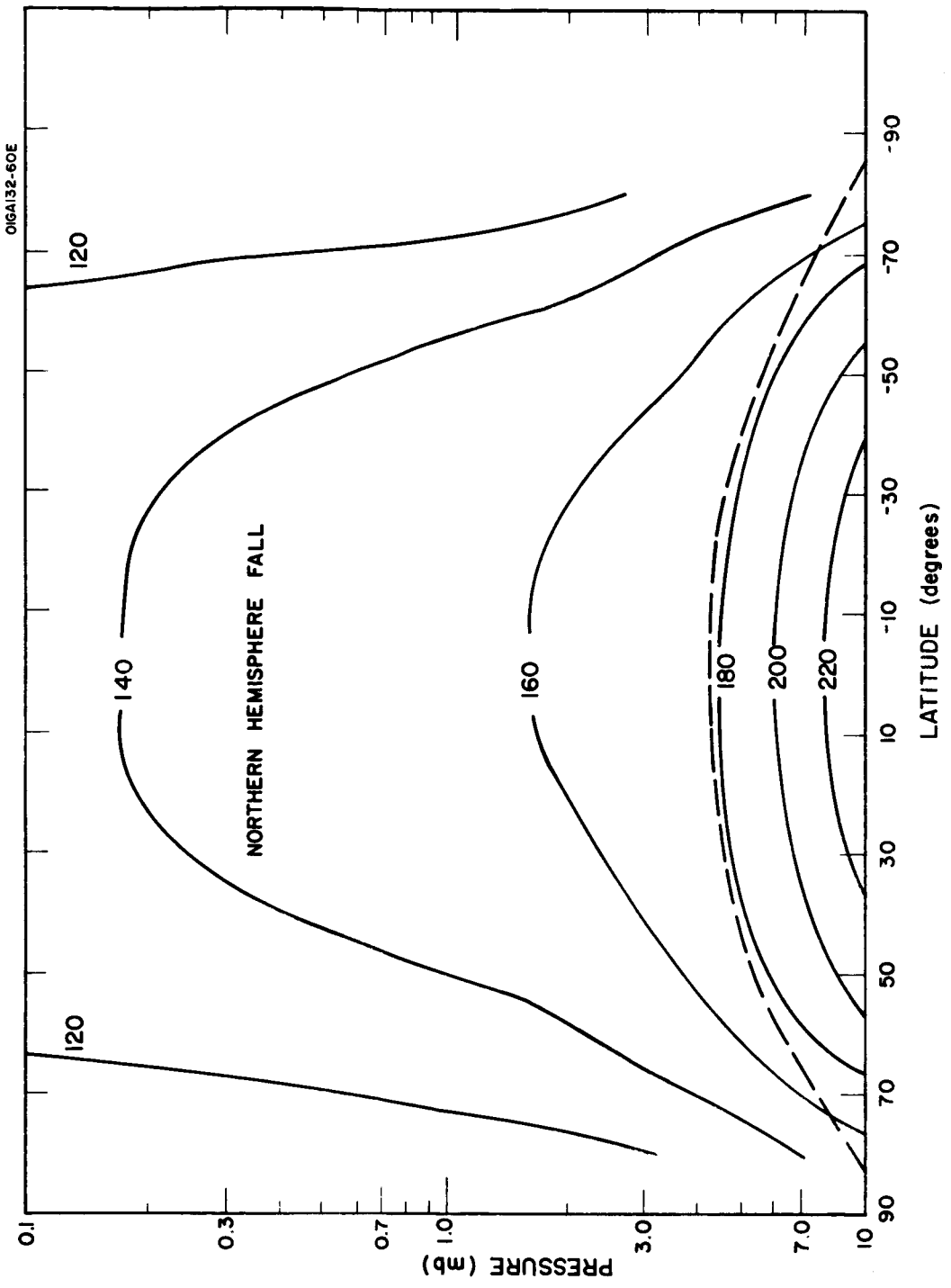

Figure 6. Computed latitudinal temperature cross-section for Northern Hemisphere fall equinox on Mars. Temperatures in ^{o}K; tropopause indicated by dashed line.

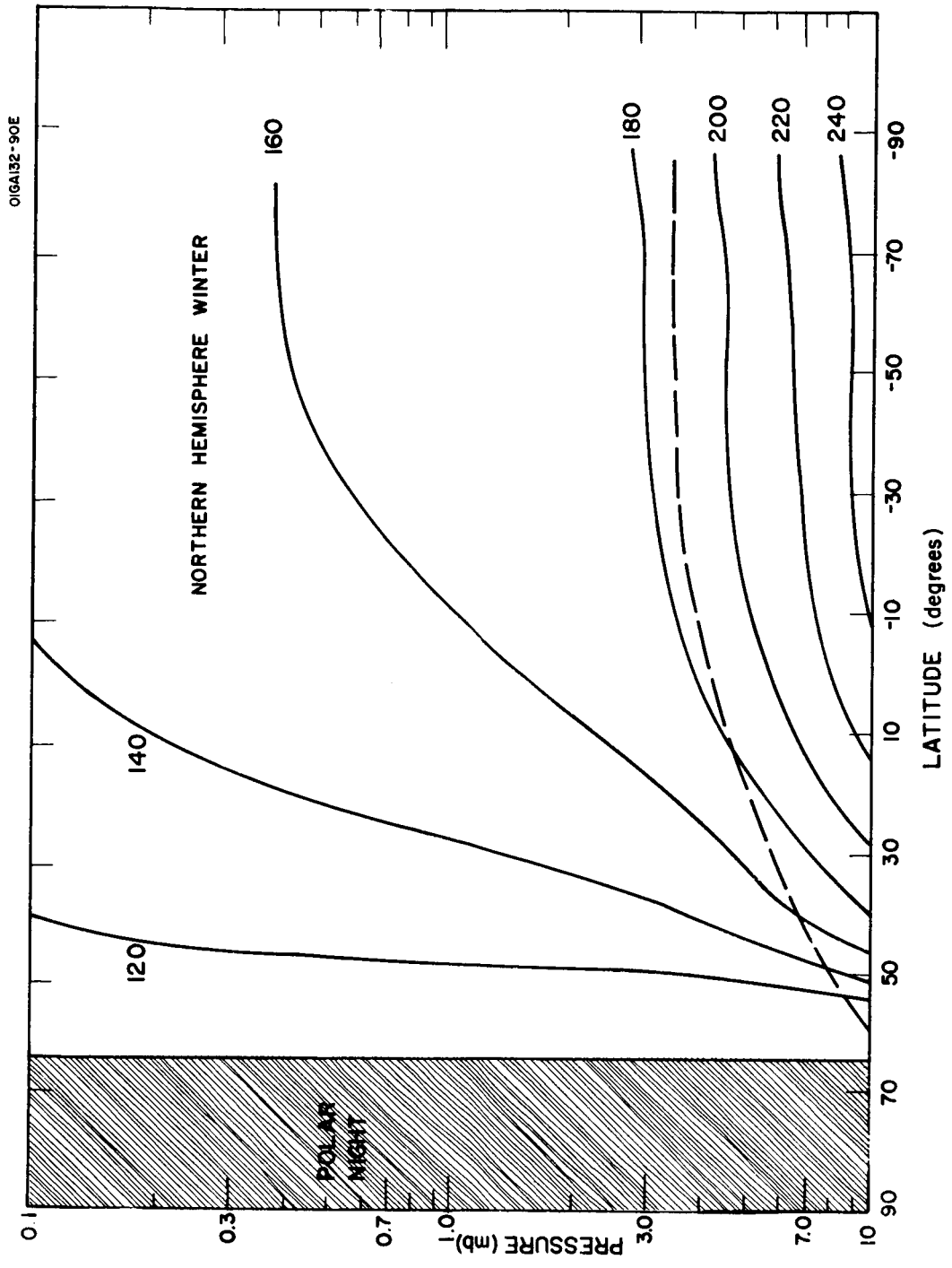

Figure 7. Computed latitudinal temperature cross-section for Northern Hemisphere winter solstice on Mars. Temperatures in ^{o}K; tropopause indicated by dashed line.

Before describing the features of the computed temperature distributions, we should discuss the representativeness of these computed temperatures. The major heat transport processes not included in the model are latitudinal transport of heat by the atmospheric circulation and conductive exchange between the planetary surface and the subsurface. The atmospheric circulation would transport heat from the regions of maximum insolation (equinoctial equator or summer pole) to the regions of minimum insolation (equinoctial poles and winter pole). The effect of such transport would be a decrease of temperature at equatorial latitudes during the equinoxes and at polar latitudes during summer, and an increase of temperature at polar latitudes during the equinoxes and in winter. The effect of conductive exchange between the surface and subsurface would be similar. Downward heat conduction into the subsurface would lower the temperature at points with maximum insolation. Upward heat conduction to the surface would raise the temperature at points of minimum insolation. Of these two processes, the effect of latitudinal transport of heat energy by the circulation is probably much more important. Smagorinsky et al (1965) obtained excellent agreement between computed and observed temperatures for the Earth's atmosphere with a model that includes the effect of the circulation but neglects conductive heat exchange.

Another heat transfer mechanism - release of latent heat due to changes of phase of CO_2 - would become important at high latitudes if the Martian polar caps are composed of solid CO_2 (Leighton and Murray, 1966; Leovy, 1966). This mechanism would tend to increase the surface temperature during the period that the cap is forming and decrease the surface temperature during the period that the cap is melting. The effect of the possible condensation of CO_2 is not allowed for in the present model.

From the above discussion we may conclude that the computed temperatures are probably somewhat too high at equatorial latitudes during the equinoxes and at polar latitudes during the summer. They are too low at polar latitudes during the equinoxes and during winter. The computed temperatures should be most representative at middle latitudes during the equinoxes and at equatorial latitudes during the solstices.

The major features of the computed temperature cross-sections are:

1. The extremely small latitudinal temperature gradients in the summer hemisphere, with the maximum temperature occurring at the pole.

2. The decrease of tropopause altitude - dashed line - with latitude from a maximum at the equator during the equinoctial seasons and at the summer pole during the solstices.

3. The relatively isothermal vertical structure at high latitudes during the equinoxes and in winter.

The average planetary surface temperatures for the four seasons are listed in Table 2. The temperature differences between the two equinoxes and between the two solstices are due to differences in the planet's distance from the sun.

It is of interest to compare the computed temperatures with observational indications of Martian temperatures and with other theoretical estimates. Indications of surface temperature are available from microwave and infrared observations. Unfortunately, both the infrared and microwave observations are of the sunlit side of the planet and therefore are representative of daytime temperatures rather than the average daily temperatures that are computed in our model. However, the microwave observations refer to temperatures at levels a few centimeters below the surface. At such levels, the effect of diurnal temperature variations would be minimal, and the observed temperatures may be close to the daily average temperatures. Unfortunately, the microwave observations do not resolve the disk. Thus, to make a comparison we must average our computed surface temperatures to obtain a planetary average surface temperature. This temperature can then be compared with the microwave observations. Our computed planetary average surface temperature is $208^{o}K$. The microwave observations yield an average temperature of about $215^{o}K$ to $220^{o}K$, when corrected for a surface emissivity of 0.89 and normalized to a mean Mars-sun distance (Dent et al, 1965; Hughes, 1966; Kellerman, 1966). The uncertainty in this temperature, due to observational errors, is about $\pm$ 5%. The agreement between the computed and observed planetary average temperature can be considered excellent.

Theoretical calculations of the latitudinal and seasonal distributions of the diurnal variation of Martian surface temperature have been performed by Leovy (1966) and Leighton and Murray (1966). Figures 8 and 9 show comparisons of our computed surface temperatures with the daily average surface temperatures of Leovy. Leovy models the atmospheric radiative exchange in a fashion similar to but simpler than ours. His treatment of convection is somewhat different from ours and he also includes the effect of conductive heat transfer between surface and subsurface. His computations are for a 5 mb surface pressure, 100 percent CO_2 atmosphere with an albedo that varies with latitude and whose average value is about 0.23. Because of a generally lower albedo, his surface temperature should be a few degrees lower than ours. However, the results are in excellent agreement except at polar regions during the equinoxes and winter. When Leovy's surface temperature falls below the condensation temperature of CO_2 ($\sim 145^{o}K$), he permits atmospheric CO_2 to condense. The release of latent heat of condensation maintains the polar temperatures during these seasons at $145^{o}K$. This effect is not included in our computations.

A comparison of our computed latitudinal distribution of annual surface temperature with that of Leighton and Murray (1966) is shown in Figure 10. Leighton and Murray parameterize the exchange of heat energy between the surface and atmosphere, but do include the effects of conductive

Table 2

Average planetary surface temperatures.

Season	Average Planetary Surface Temperature (^{o}K)
Northern Hemisphere Spring Equinox	210
Northern Hemisphere Summer Solstice	194
Northern Hemisphere Fall Equinox	217
Northern Hemisphere Winter Solstice	212

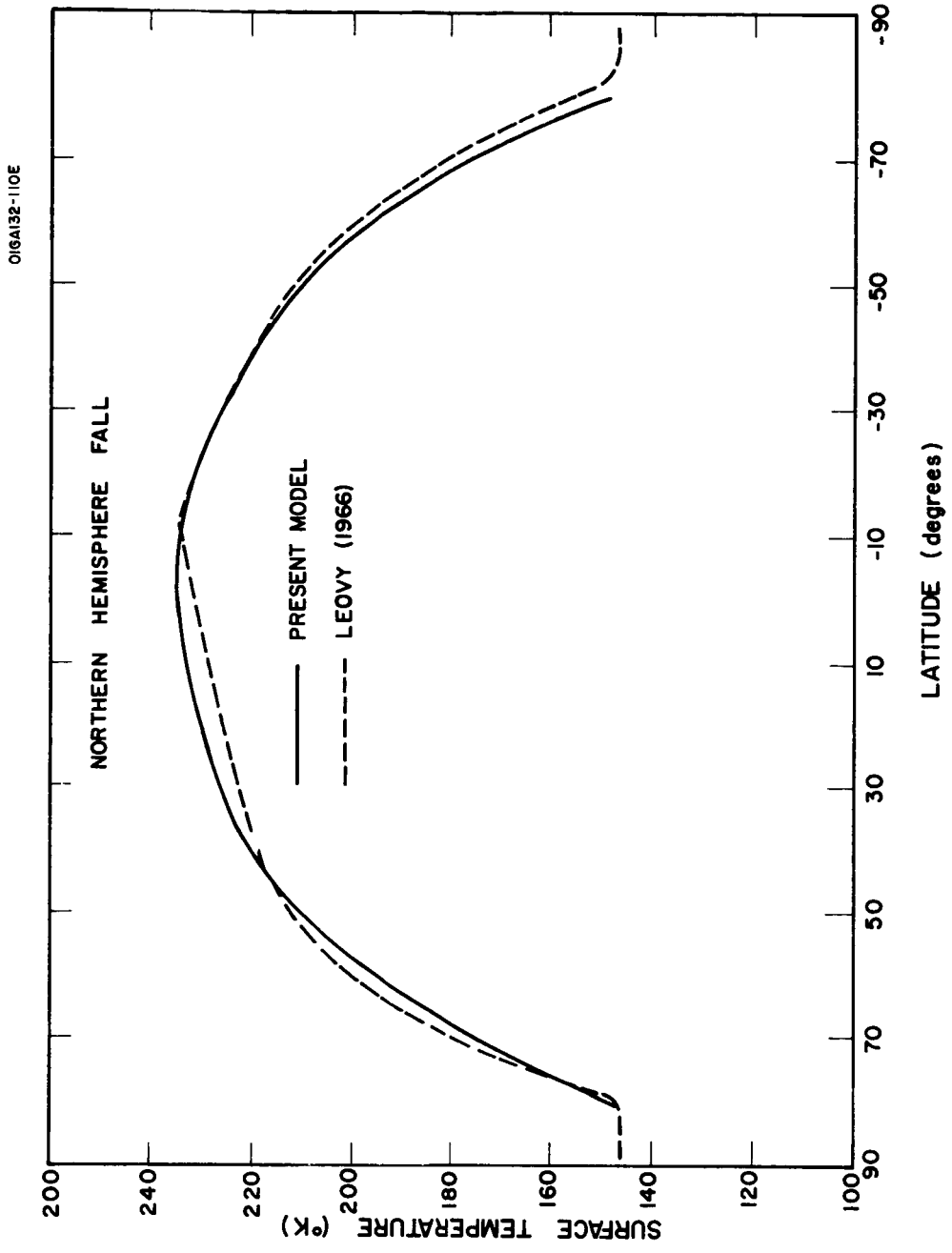

Figure 8. Comparison of computed latitudinal variation of Martian surface temperature for Northern Hemisphere fall equinox with that of Leovy (1966). Solid line - present model; dashed line - Leovy (1966).

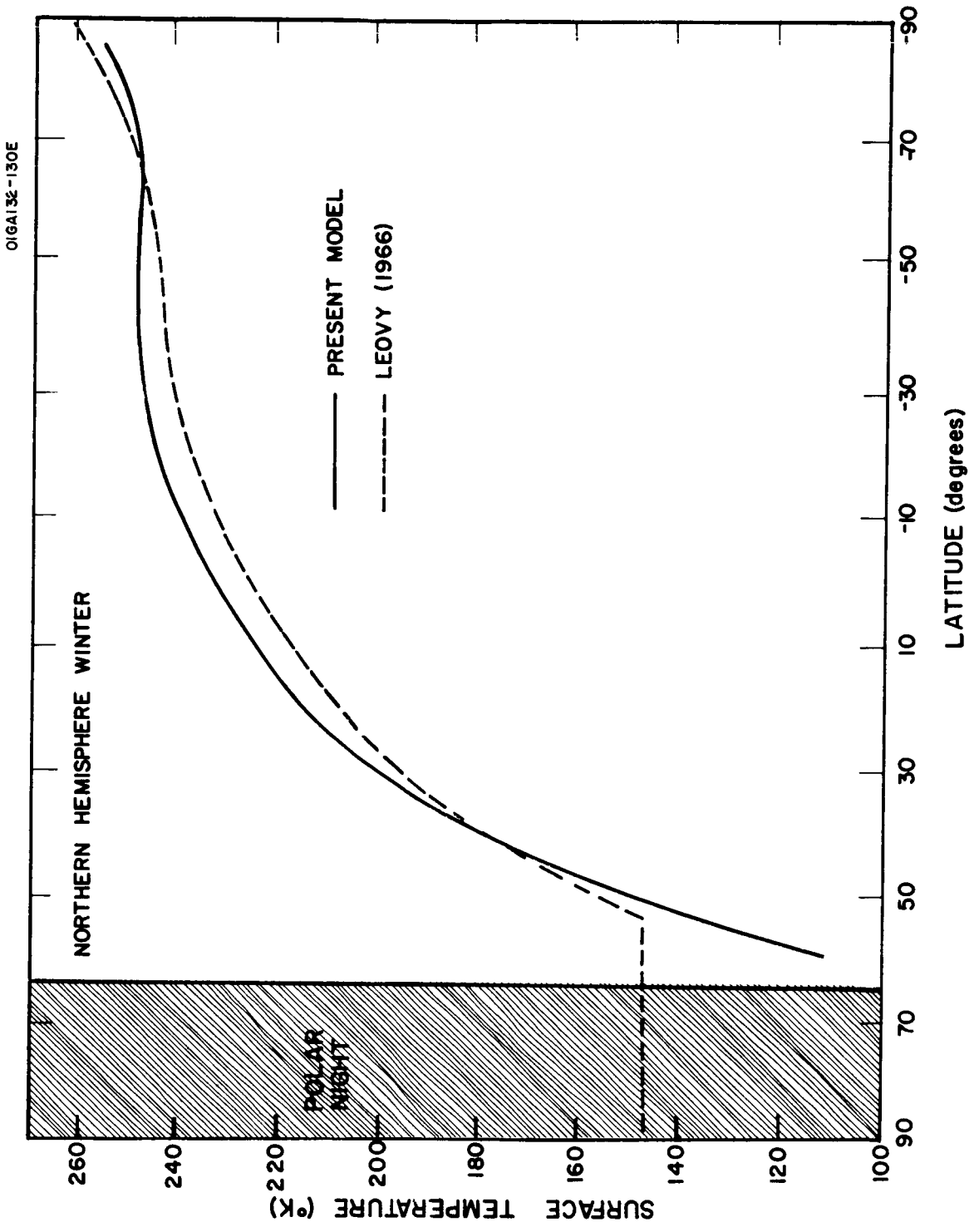

Figure 9. Comparison of computed latitudinal variation of Martian surface temperature for Northern Hemisphere winter solstice with that of Leovy (1966). Solid line - present model; dashed line - Leovy (1966).

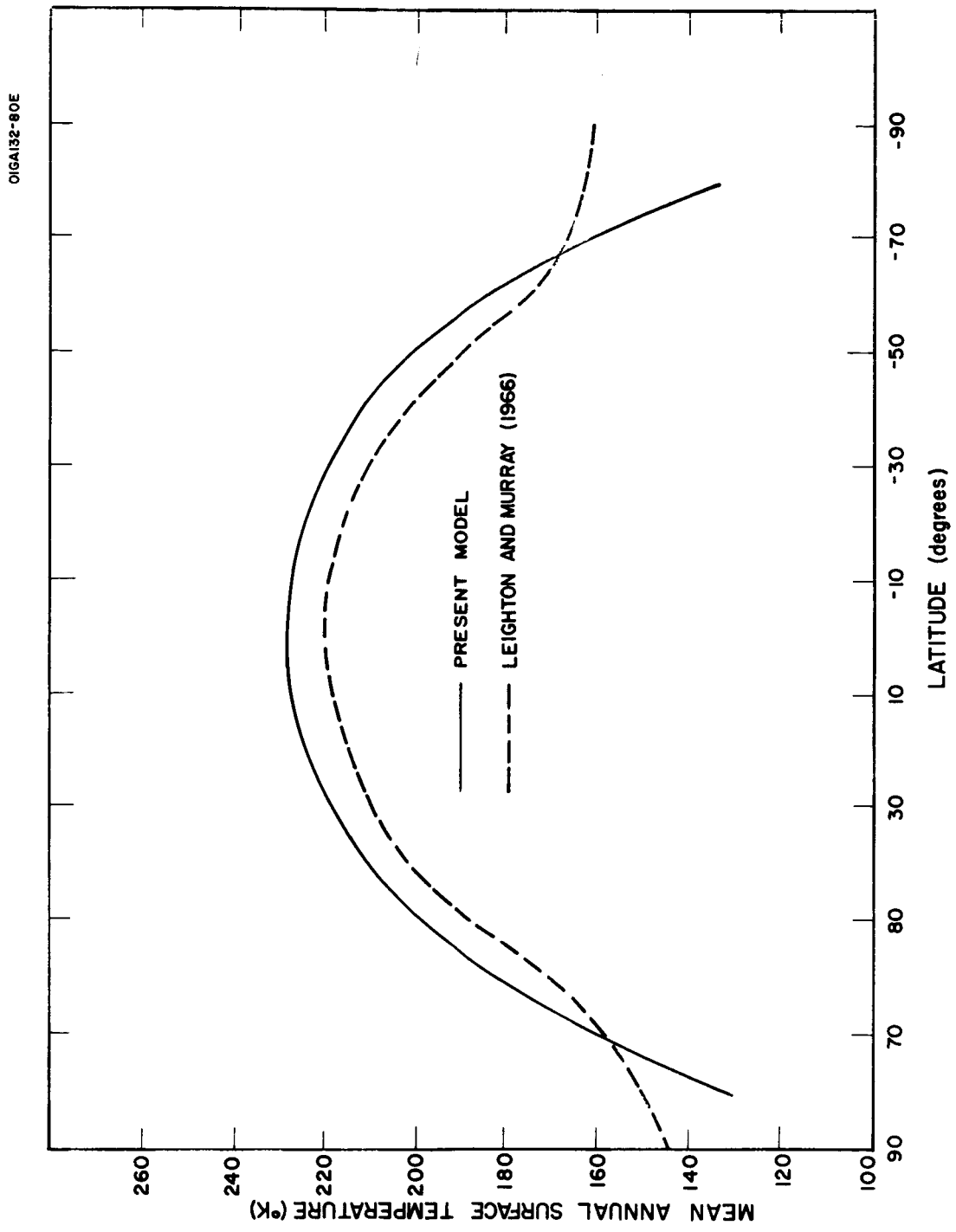

Figure 10. Comparison of computed latitudinal variation of mean annual Martian surface temperature with that of Leighton and Murray (1966). Solid line - present model; dashed line-Leighton and Murray (1966).

heat exchange between surface and subsurface and the effect of the release of latent heat due to condensation of CO_2. Their assumed albedo is 0.15. The comparison indicates that their temperatures are some 8 to 10°K lower than ours at low and middle latitudes. Since their assumed albedo is lower than ours, their computed temperatures should not be lower but higher than ours at these latitudes. The reason for the discrepancy may be their simplified modelling of heat exchange between surface and atmosphere. Their polar temperatures are higher than ours because they include the effect of condensation of atmospheric CO_2. Generally speaking, the results of all three theoretical models - ours, Leovy's, and Leighton and Murray's - are in excellent agreement on the latitudinal variations of surface temperature.

There is no observational information available on the latitudinal and seasonal variations of the Martian vertical temperature distribution with which to compare our results. There are also no theoretical estimates except those from Leovy's (1966) two layer atmosphere model. In Figures 11 and 12 we compare our latitudinal distributions of computed temperature at the atmospheric level, $p/p_o = 0.31$, where p is pressure and p_o is surface pressure, with those of Leovy for the same atmosphere level. In general, our computed temperatures are generally 20°K to 35°K lower than Leovy's. The reason for this difference is not immediately obvious. It may be that Leovy has overestimated the convective heat flux, which would lead to higher atmospheric temperatures and lower surface temperatures in his model. This would also explain why his surface temperatures agree quite well with ours despite his lower albedos.

A rough comparison can be made between our computed temperatures and the temperatures inferred from the Mariner IV occultation experiment.

Figure 13 shows a temperature profile computed for the latitude and time of year at which the Mariner IV occultation experiment during immersion was performed. Immersion occurred at 50°S latitude in late winter at a local time of 1 P.M. when the solar zenith angle was 67°. Our computations were performed for 50°S latitude and solar declination angle of +15° (corresponding to the day of the occultation measurement). The temperature near the surface derived from the immersion occultation experiment was 175°K ± 25°K (Kliore et al, 1965). This is presumably an average temperature of the lower Martian atmosphere. In addition, it was found that there was no obvious change of scale height with altitude in the first 30 km. Our calculations indicate a surface temperature of 173°K and a decrease of temperature with altitude to less than 120°K at p = 0.1 mb (~ 40 km). Our average temperature (pressure weighted) for the first 40 km would be about 150°K. Two factors would cause the computed temperatures to be less than the actual temperatures. The present computation represents the average diurnal temperature for the day and location of encounter. One would expect the average diurnal temperature to be less than the 1 P.M. temperature, which should be close to the maximum daily temperature. In addition, latitudinal heat transport is neglected

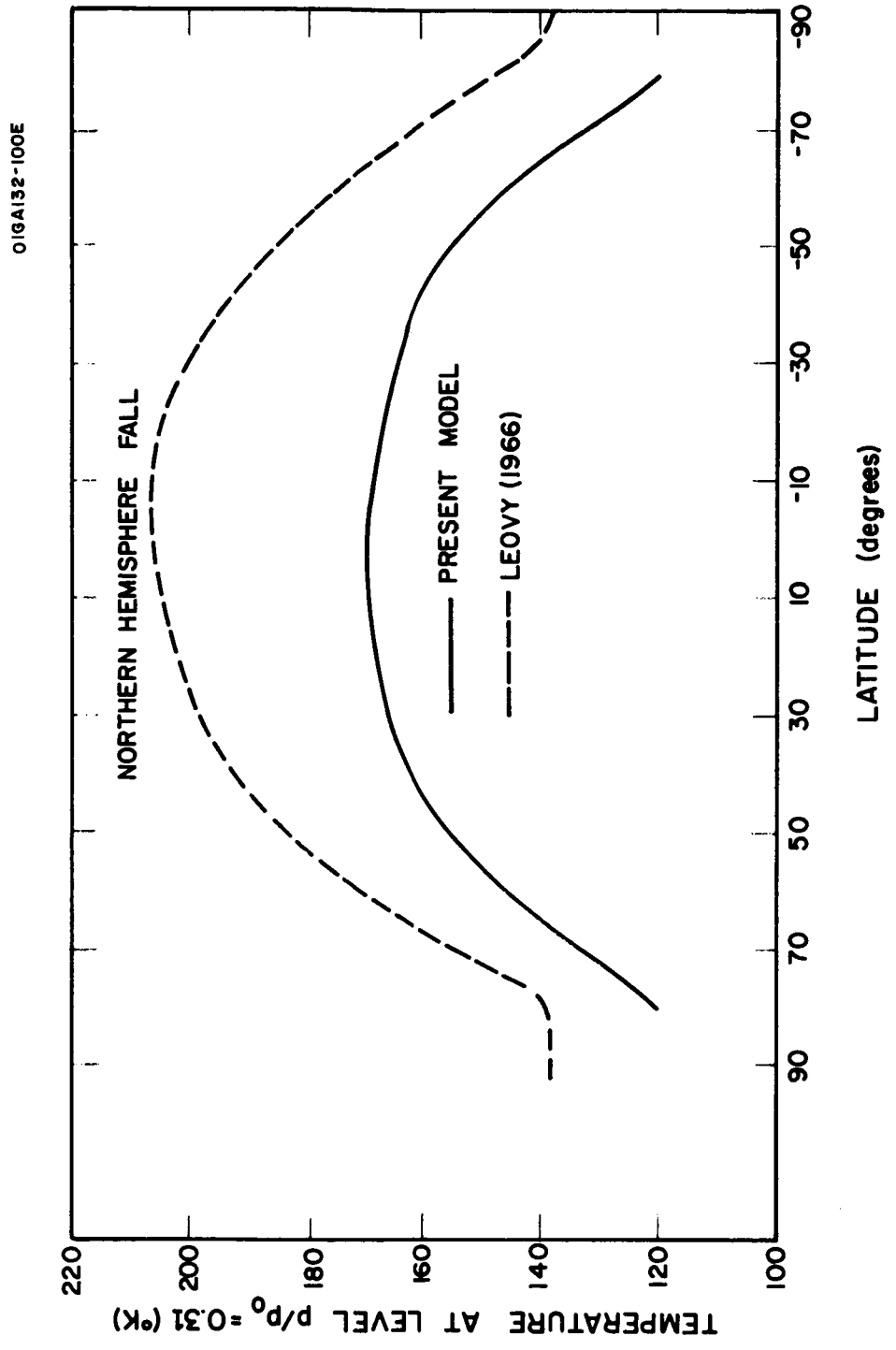

Figure 11. Comparison of computed latitudinal variation of Martian temperature at atmospheric level $p/p_o=0.31$ for Northern Hemisphere fall equinox with that of Leovy (1966). Solid line-present model; dashed line - Leovy (1966).

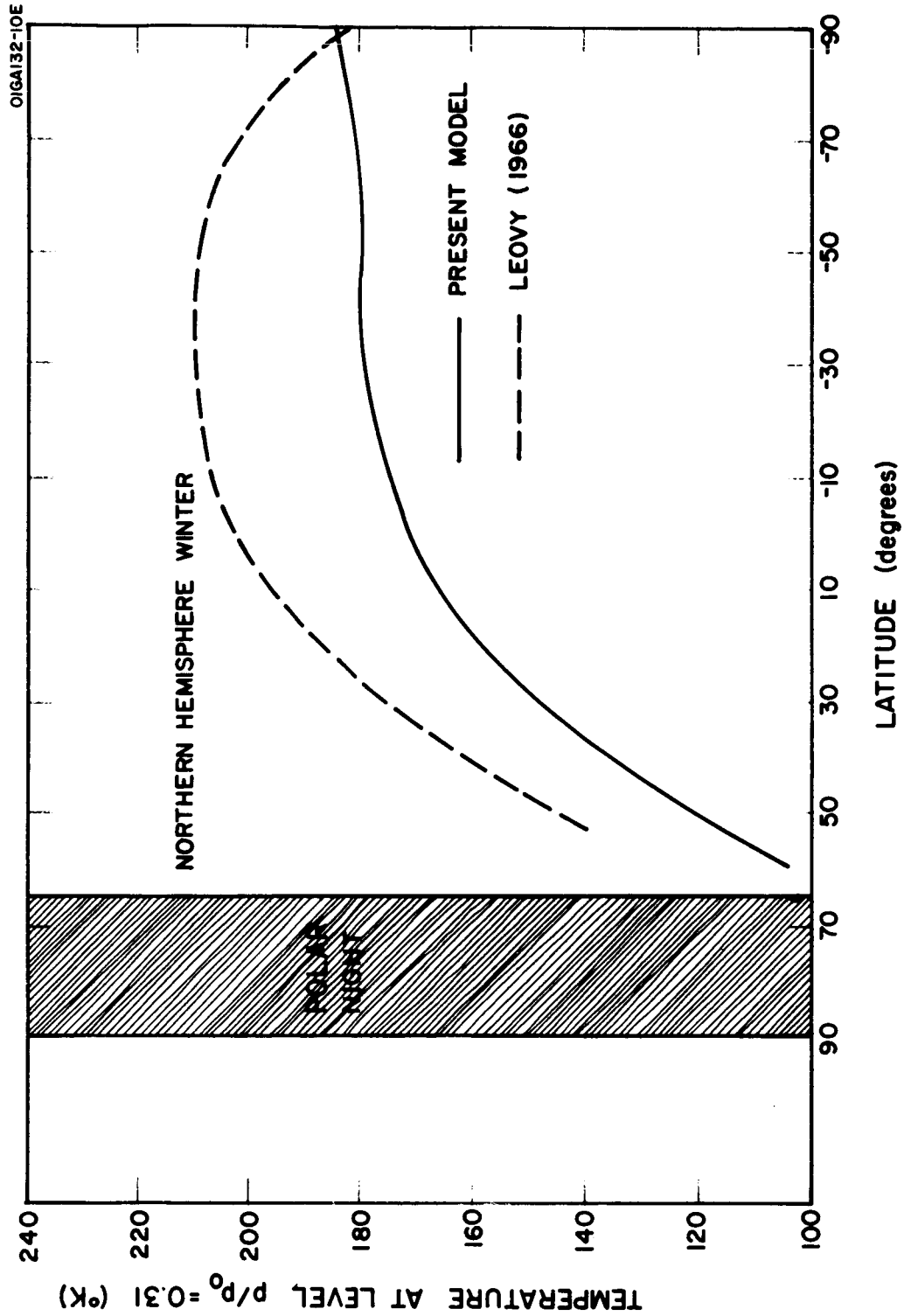

Figure 12. Comparison of computed latitudinal variation of Martian temperature at atmospheric level $p/p_o=0.31$ for Northern Hemisphere winter solstice with that of Leovy (1966). Solid line - present model; dashed line - Leovy (1966).

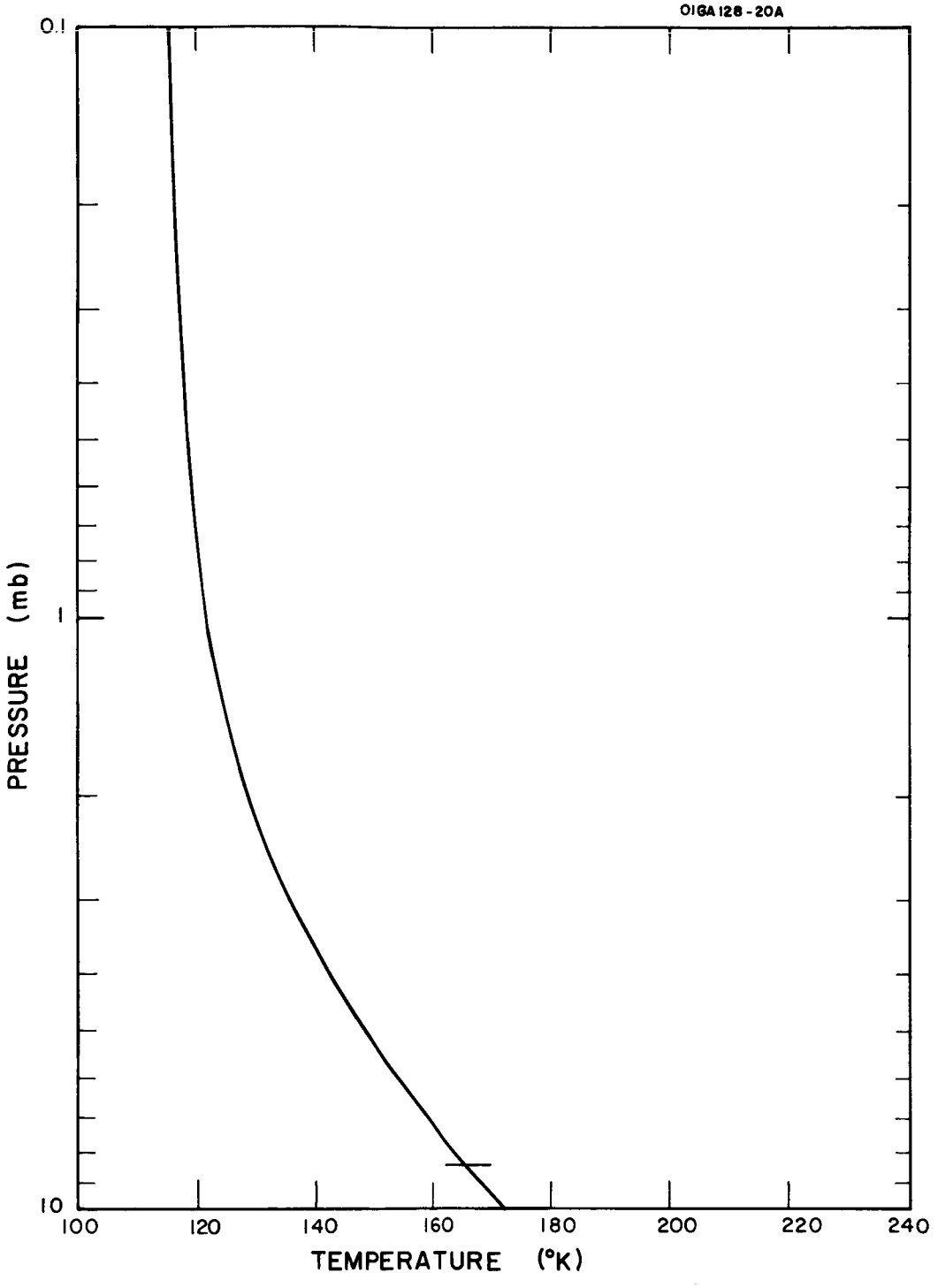

Figure 13. Computed temperature profile of the Martian atmosphere for the date of the Mariner IV immersion occultation experiment (50°S, solar declination +15°, late Southern Hemisphere winter).

in the model. At this latitude during winter, one would expect latitudinal heat transport to increase the computed temperatures somewhat. An addition of 20°K to our computed values would be a reasonable correction for these effects and would place the computed temperature in excellent agreement with temperature derived from the immersion experiment. However, our computed temperatures do suggest that the scale height would vary by about 30 percent from the surface to about 40 km, which is not in agreement with the immersion observations.

Figure 14 shows a computed temperature profile for the latitude and solar declination on the day of emmersion, which occurred at 60°N at night during late summer. According to Kliore et al (1966) the temperature at emmersion was 220°K and according to Fjeldbo et al (1966) the apparent lapse rate was greater at emmersion than on immersion. Our calculations indicate a surface temperature of 222°K and a decrease of temperature with altitude to less than 135°K at 1.0 mb. Our average temperature for the first 40 km would be about 180°K. Since at the local time, season, and latitude of emmersion, both diurnal effects and latitudinal heat transport processes would tend to decrease our computed temperatures, it must be concluded that the computed temperatures for emmersion are not in good agreement with the observed temperature on emmersion. Our results for emmersion do indicate a greater lapse rate in the first 30 km, in agreement with the observations.

Whether the thermal equilibrium temperature profile is a good estimate of the actual daily average temperature profile for a particular time of year may be questioned on the grounds that a certain amount of time is necessary for an initial temperature profile to become a thermal equilibrium temperature profile. It will be recalled that, in computing the thermal equilibrium temperature, an initial temperature profile begins the iterative process of the computational model and, after a certain number of iterations, the final temperature profile is approached. Thus, the equilibrium temperature profile is the steady state solution to the convective and radiative equations governing the temperatures in the Martian atmosphere, which is approached asymptotically through the iterative cycles of the computational model. In the computational model all the atmospheric parameters (i.e. surface pressure, CO_2 mass mixing ratio, solar insolation, etc.) remain constant during the time required to reach equilibrium. In the actual case, the one atmospheric parameter that definitely changes with time is the average solar insolation. In our computations, it was implicitly assumed, however, that this change was negligibly small during the time necessary for a given initial temperature profile to approach asymptotically the steady state, thermal equilibrium temperature profile. The validity of this assumption was studied in the following manner.

Starting with a thermal equilibrium profile for a particular latitude and time of year, we computed temperature profiles at successive 10-day time steps for an annual cycle using the basic computational model to

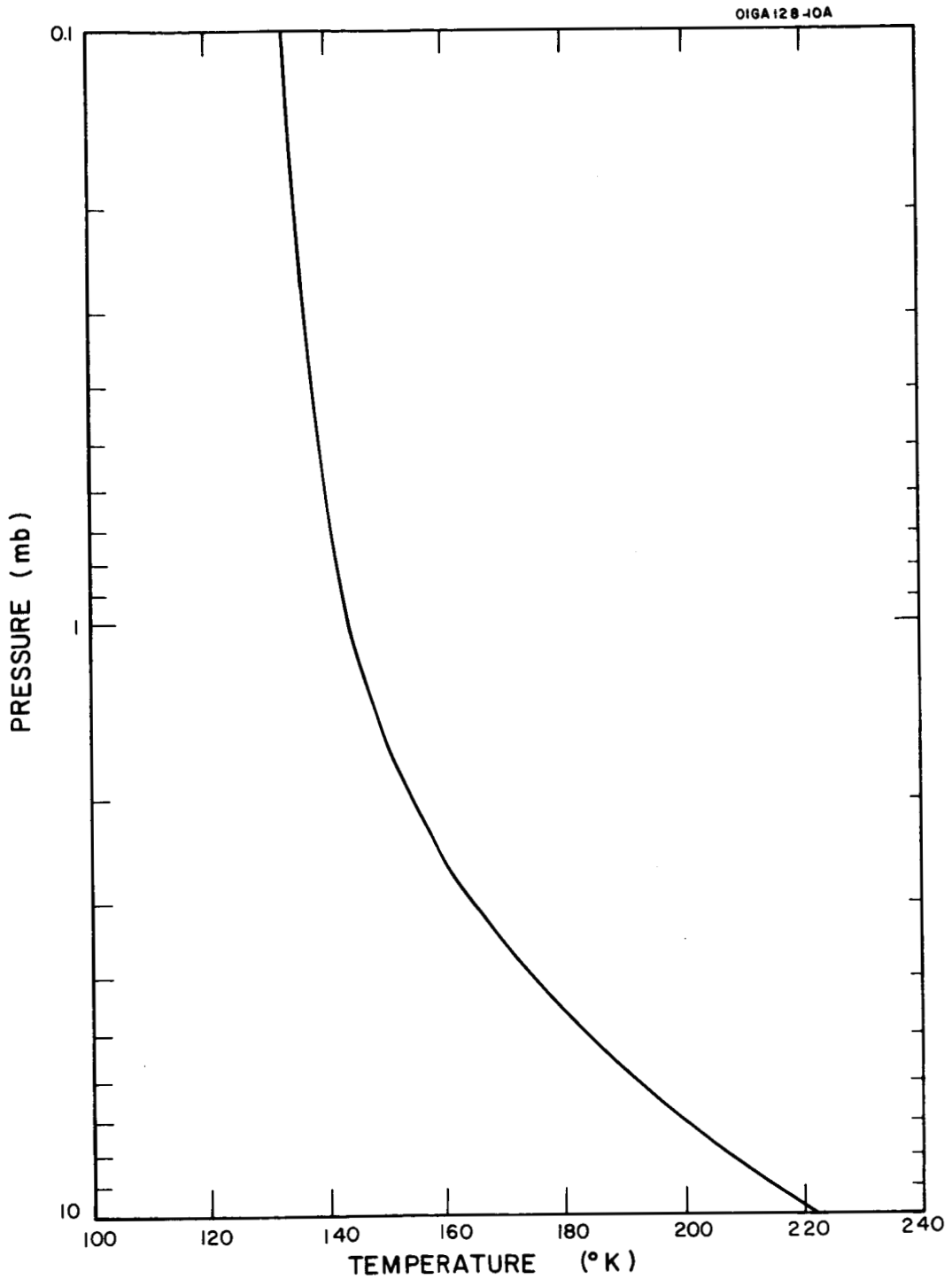

Figure 14. Computed temperature profile of the Martian atmosphere for the date of the Mariner IV emmersion occultation experiment (60°N, solar declination +15°, late Northern Hemisphere summer).

determine the change in temperature during a single time step of 10 days. From one time step to the next the average solar insolation changes such that during the τ-th time step, the average solar insolation is given by

$$\bar{S}_o\ (\tau) = \tfrac{1}{2}\ [\ S_o(\tau) + S_o(\tau\text{-}1)\ ]$$

where $S_o(\tau)$ and $S_o(\tau\text{-}1)$ are the average solar insolations at the end and beginning of the 10-day period of the τ-th time step. The temperatures computed in this manner can then be checked against the thermal equilibrium temperatures.

Computations were performed for Martian latitudes 0^o and 80^oN. The initial temperature profiles were the thermal equilibrium temperature profiles for the Northern Hemisphere spring equinox and for a date 45 days before the Northern Hemisphere spring equinox, respectively. Figures 15 and 16 are graphs of the daily average surface temperature as a function of time for 0^o and 80^oN respectively. Included in Figures 15 and 16 are the respective thermal equilibrium surface temperatures for the first day of the four Martian seasons. (Only 3 seasons appear in Figure 16, as the Northern Hemisphere winter solstice occurs during the polar night.)

As can be seen, the thermal equilibrium surface temperatures are in excellent agreement with the "time dependent" surface temperatures except at 80^oN during the spring and autumnal equinoxes, when a maximum temperature difference of about 25^oK occurs. Therefore, the computed equilibrium temperature profiles should give reasonable estimates of the seasonal variations of Martian temperatures.

1.8 Concluding Remarks

Martian pole-to-pole temperature cross-sections from the surface to about 40 km altitude for each season have been computed with a thermal equilibrium model. The computed average temperatures should be closest to the actual average temperatures at middle latitudes during the equinoxes and at low latitudes during the solstices. Because the model does not allow for latitudinal transport of heat energy by the atmospheric circulation and the possible condensation of carbon dioxide, the computed temperatures are too low at polar latitudes during the equinoxes and winter and probably too high at equatorial latitudes during the equinoxes and at polar latitudes during summer. The major features of the computed temperature cross-sections are:

(1) The extremely small latitudinal temperature gradients in the summer hemisphere, with the maximum temperature occurring at the pole.

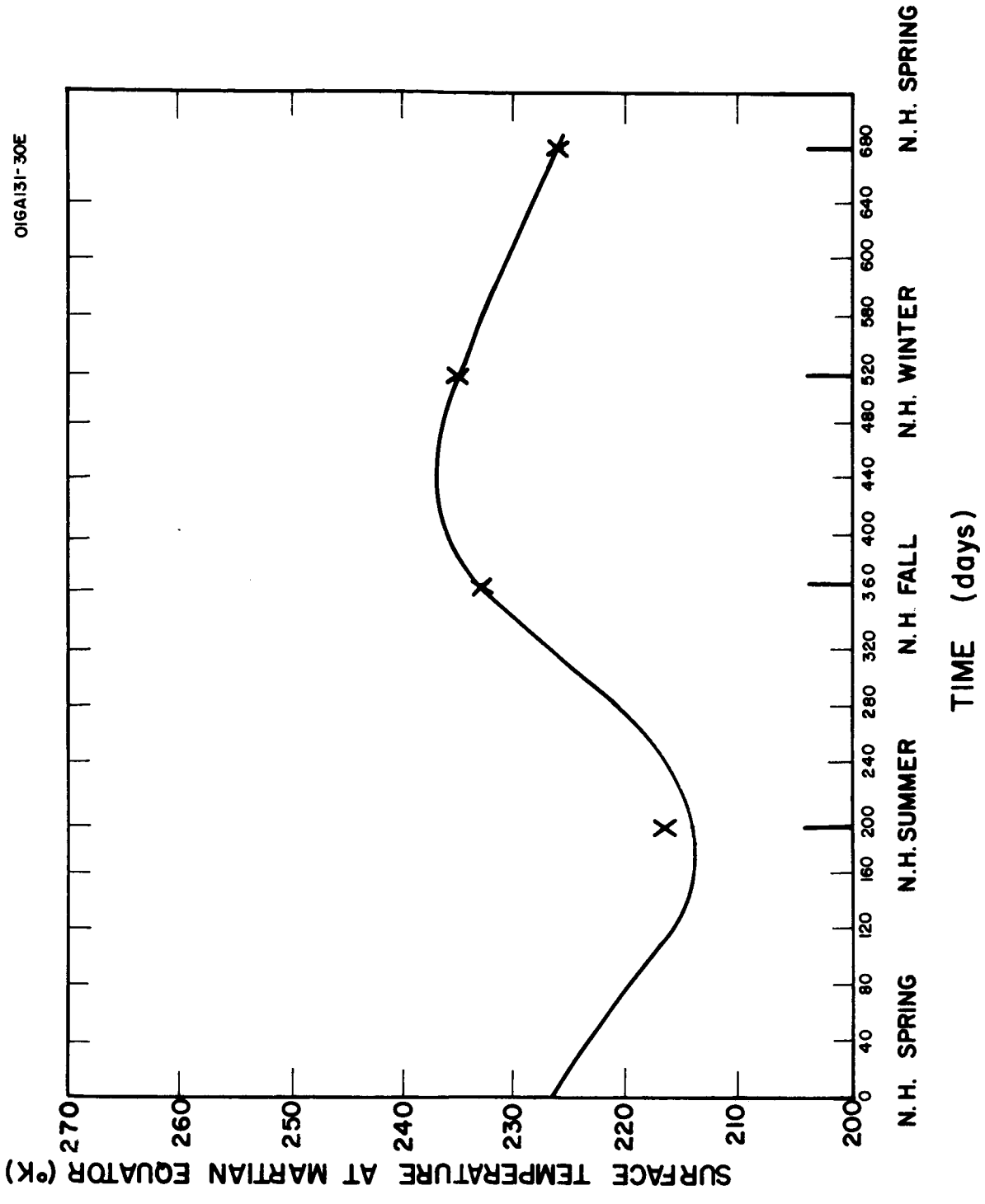

Figure 15. Martian surface temperature as a function of time at equator. Solid line: time dependent case starting with initial thermal equilibrium condition at Northern Hemisphere spring equinox. X: computed on basis of thermal equilibrium.

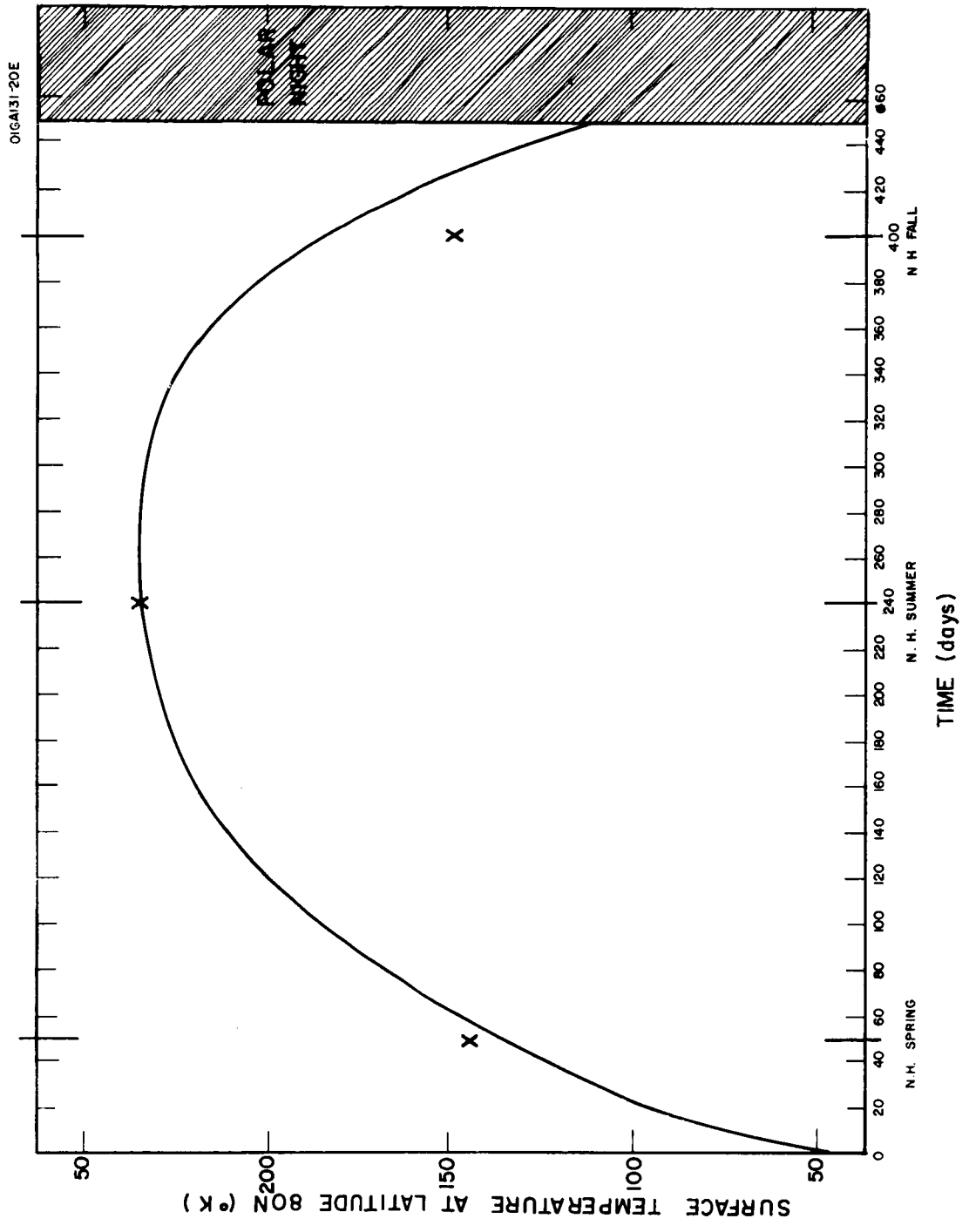

Figure 16. Martian surface temperature as a function of time at 80°N. Solid line: time dependent case starting with initial thermal equilibrium condition at 45 days prior to spring equinox. X: computed on the basis of thermal equilibrium.

(2) The decrease of tropopause altitude with latitude from a maximum at the equator during the equinoctial seasons and at the summer pole during the solstices.

(3) The relatively isothermal vertical structure at high latitudes during the equinoxes and winter.

Comparisons of the present results with other theoretical studies and with the microwave and Mariner IV observations of Martian temperatures yield generally good agreement. Further theoretical studies of temperatures of the surface and lower atmosphere of Mars should include the effects of latitudinal heat transport, release of latent heat of condensation, conductive heat exchange between surface and sub-surface, atmospheric water vapor radiative transfer, and analyses of the diurnal temperature wave.

2. THE GENERAL CIRCULATION OF THE MARTIAN ATMOSPHERE

Wen Tang

2.1 SEASONAL VARIATIONS OF THE MEAN ZONAL WIND VELOCITY AND TEMPERATURE OF THE MARTIAN ATMOSPHERE

2.1.1 Introduction. More than one and half decades ago, the general circulation of the Martian atmosphere was essentially inferred from telescopic observations of the movement of yellow clouds and radiometric observations of the surface temperature (Hess and Panofsky, 1951). In 1961, Mintz applied dynamic stability theory to the Martian atmosphere to determine the type of general circulation on the planet — symmetric or wave type.

Recently, Tang (1966) used the new data on atmospheric composition and surface pressure (Kliore, 1966) and a general circulation model for steady state and symmetrical regime to study the mean zonal and meridional winds in the northern hemisphere and the stability of the symmetrical regime in the Martian atmosphere during the equinoctial seasons. The purpose of the present work is to study the seasonal mean zonal winds and temperatures at the middle of the Martian atmosphere with the use of a simple dynamic model.

2.1.2 General Theory. Based upon the principle of conservation of energy, Adem (1962) developed a simple model of the general circulation for the Earth's atmosphere. His model yields mean monthly meridional profiles of zonal wind and temperature that agree well with observed mean profiles. We can apply this model to Mars.

We shall outline the concept involved in this model. For the details of the theory and the basic mathematical developments we refer the reader to Adem (1962). If the constituents of the atmosphere and the temperature are known, the energy emitted from an atmospheric layer can be calculated. From the balance of radiational energy, one can evaluate the excess of radiational energy at an atmospheric level and at the surface, if the atmospheric and surface temperatures, insolation, and albedo are known. Conversely, the atmospheric and surface temperatures can be computed if the excesses of both atmospheric and surface radiation energy are known. Two equations with four unknows arise from writing down the radiation budget equations for the surface and atmosphere. Two more equations are needed to determine these quantities uniquely. One of these two is the energy equation, which essentially indicates that the rate of change of thermal energy due to meridional turbulent transport is equal to the rate of change of thermal energy due to radiation plus the rate of change of conduction of sensible heat and the molecular transformation. The fourth equation may be considered as an empirical equation which is used to evaluate some unknown with observational data. With these four equations the meridional profiles of the temperature for different seasons can be determined. By using the geostrophic wind equation, the meridional profile of mean zonal wind can be obtained from the computed meridional temperature profile.

The final governing equation for the latitudinal variation of atmospheric temperature is (Adem, 1962)

$$\frac{d^2}{d\varphi^2}\bar{T}'_m + c_6^2\,\bar{T}'_m = -\frac{c_1}{c_7\bar{K}}I_d - \frac{c_o}{c_7\bar{K}} + \frac{J - c_4\bar{E}_3}{c_7\bar{K}} \qquad (55)$$

where

$\bar{T}'_m$ = the deviation of mean atmospheric temperature at latitude φ from the mean atmospheric temperature at a given latitude for a given season.

φ = Latitude

I_d = The insolation during one day

J = The rate of change of the conduction of sensible heat and the molecular transformation function.

$\bar{E}_3$ = The excess mean radiational energy at the surface of Mars.

$c_6 = (1-Ac_2)/c_7\bar{K}$

$\bar{K}$ = Eddy viscosity

$c_7 = -c_3(A_1)(1 + \beta A/2)/r_o^2$

r_o = Radius of Mars

$A_1 = c_v/2\,(p^*_{o\ z=0} - p_o)$

$A = 2H_o/(4T_o+\beta H_o)$

p_o = Pressure

c_v = Specific heat at constant volume

g = Gravitational acceleration of Mars

H_o = Height of the top of the absorbing gases

T_o = The temperature at height H_o

β = The mean lapse rate

and

c_o, c_1, c_3, and c_4 = coefficients of the following equation

$$(1-A)\ \bar{T}'_m = c_o + c_1 I_d + c_3 \bar{E}_A + c_4 \bar{E}_s \tag{56}$$

The quantity $\bar{E}_A$ is the excess of the mean radiational energy of the Martian atmosphere. The boundary conditions are that the temperature gradients both at the equator and poles are zero, that is,

$$\frac{d}{d\varphi} \bar{T}'_m = 0 \qquad \text{at} \quad \varphi = 0 \text{ and } \frac{\pi}{2} \tag{57}$$

The solution to the differential Equation (55) and boundary conditions in Equation (57) is

$$\bar{T}'_m(\varphi) = \frac{c_1}{c_6\, c_7\, \bar{K}} \left\{ \int_o^{\varphi} I_d(\psi) \sin(\psi - \varphi)\, d\psi \right.$$

$$+ \frac{1}{2} \left[\int_o^{\pi} I_d(\psi) \cosh c\, (\psi - \tfrac{\pi}{2})\ d\psi \right] \frac{(\cos c_6\varphi + \sin c_6\varphi)}{\sinh c_6\pi/2}$$

$$\left. - \frac{c_o - J}{c_6 c_1} \right\} \tag{58}$$

The quantity J is an unknown quantity. It can be evaluated by applying Equation (58) to a latitude for which we have a good estimate of the atmospheric temperature from observational or other theoretical results.

The wind field is determined from simple geostrophic wind relations. If the latitudinal temperature deviation is known, then the mean zonal and meridional wind velocity can be simply written as

$$f\,\bar{u} = -\frac{R}{r_o} \frac{\partial \bar{T}'_m}{\partial \varphi} \tag{59}$$

and

$$\bar{v} = 0$$

respectively, where f = Coriolis parameter for Mars and R = gas constant for Martian atmosphere.

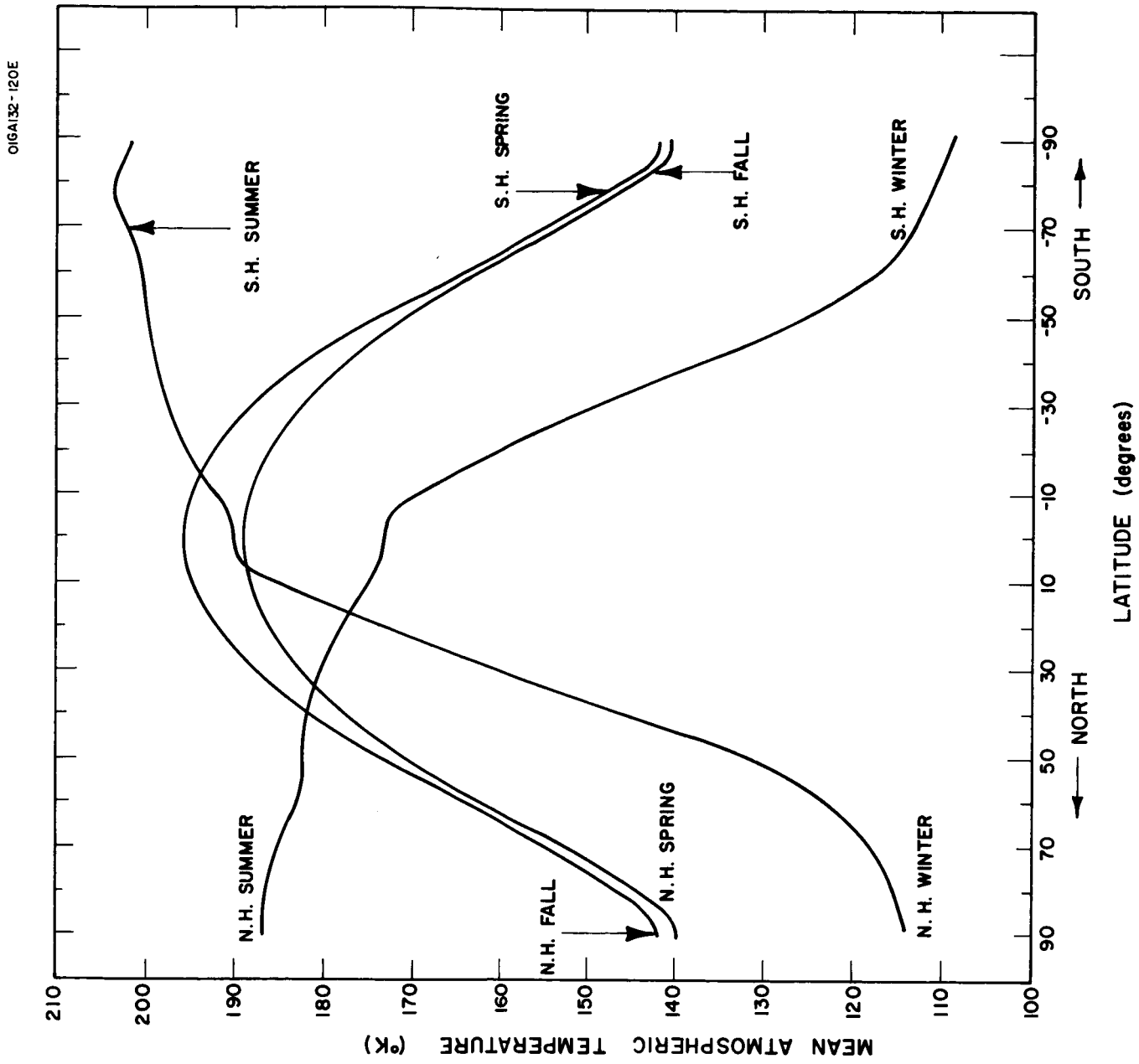

Figure 17. Latitudinal profile of mean atmospheric temperature for the four Martian seasons.

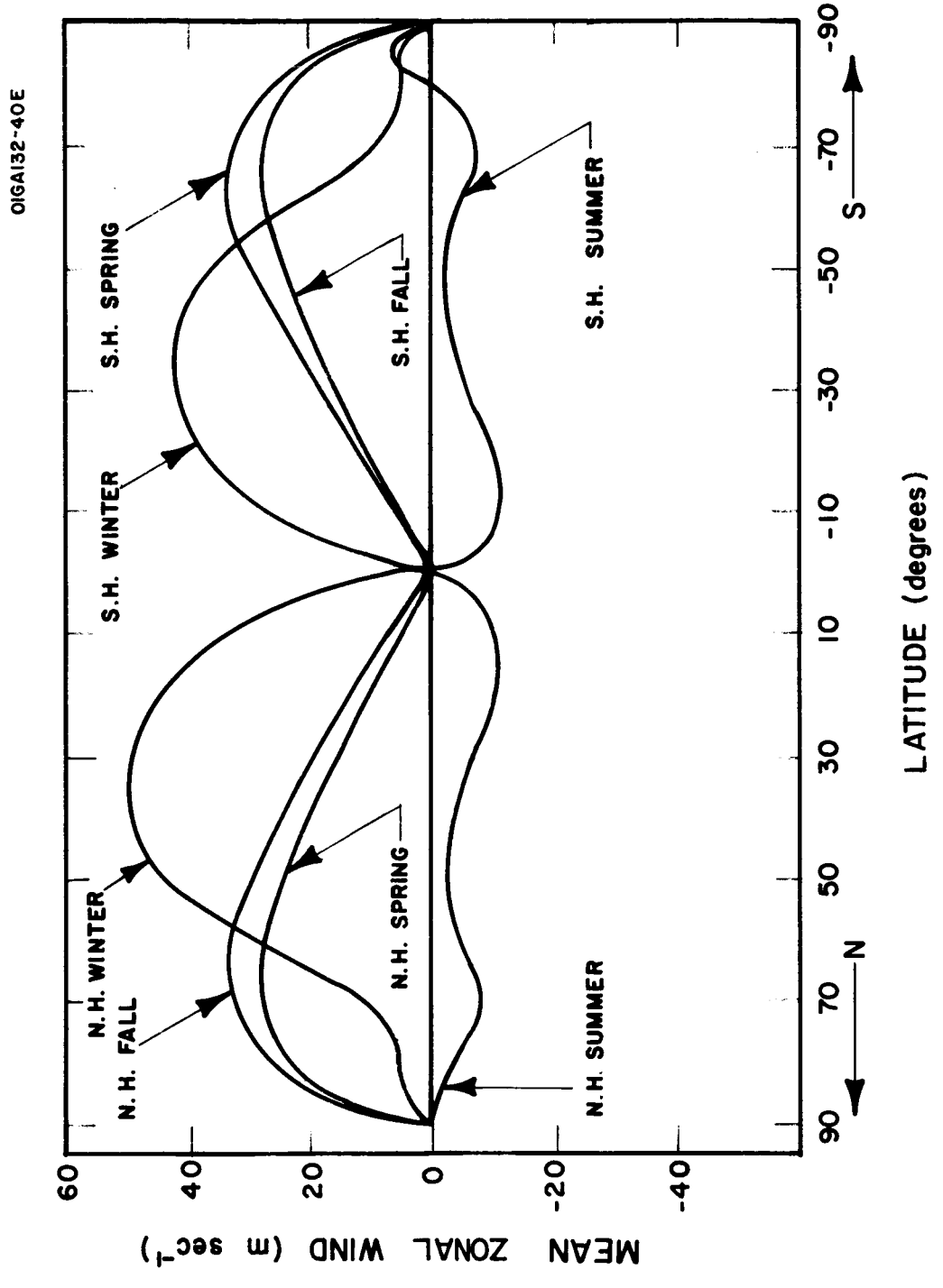

Figure 18. Latitudinal profile of mean zonal wind for the four Martian seasons.

g = Gravitational acceleration = 380 cm sec^{-2}

Ω = Angular velocity = 6.57×10^{-5} sec^{-1}

K = Eddy exchange coefficient = 10^{10} cm^2 sec^{-1}

r_o = Radius of Mars = 3400 km

c_v = Specific heat of constant volume = 0.158 cal gm^{-1} deg^{-1}

The input temperatures, $\overline{T}_N$ and $\overline{T}_S$, at 35°N and 35°S respectively, for the four seasons are as follows:

	Northern Hemisphere Winter	Northern Hemisphere Spring	Northern Hemisphere Summer	Northern Hemisphere Fall
$\overline{T}_N$(°K)	160	180	190	188
$\overline{T}_S$(°K)	205	180	145	184

The computed mean atmospheric temperature profiles for the four Martian seasons are shown in Figure 17. The extreme temperatures are found to occur in the Southern Hemisphere. The highest mean atmospheric temperature is about 205°K and occurs at 80°S during the Southern Hemisphere summer solstice. The lowest mean atmospheric temperature is about 108°K and occurs at the South Pole during the Sourthern Hemisphere winter solstice. It is interesting to note that the difference between the maximum and minimum mean atmospheric temperature, at the North Pole is smaller than the corresponding difference at the South Pole. This is a result of the planet's being closer to the sun during the Southern Hemisphere summer solstice. It is also interesting to note that the highest mean atmospheric temperature in the Northern Hemisphere occurs at the equator during the autumnal equinox. For both equinoctial seasons the mean atmospheric temperature profiles are symmetric about the equator. The temperature profiles of Figure 17 were compared to the mid-atmospheric temperatures of the thermal equilibrium model discussed in the previous section (see Figures 4 through 7). In the region bounded by the latitudes 50°N and 50°S the corresponding temperatures differ by at most 10°K. In the regions about the North and South Poles, the present temperatures are higher than the thermal equilibrium temperatures for all seasons except the summer solstice. This is due mainly to the meridional transport of heat from the warmer equatorial regions to the polar regions, which is included in the present model.

The temperatures computed from the Mariner IV occultation measurements by Kliore (1966) are about 220°K at 60°N latitude and about 175°K at 50°S latitude. These measurements were made during the late Northern Hemisphere summer (declination of sun = +15 degrees). The Mariner IV temperatures are much higher (about 40°K) than the corresponding mid-atmospheric temperatures as interpolated for

this time of year from Figure 17. If the temperatures of Figure 17 are reasonable estimates of the actual mid-atmospheric temperatures of Mars, one can conclude that the Mariner IV temperatures are representative of the atmospheric temperatures in the vicinity of the Martian surface.

The mean zonal wind profiles, based upon the geostrophic assumption, for the four Martian seasons are shown in Figure 18. The maximum mean zonal winds occur at latitudes 35°N and 35°S during the Northern Hemisphere winter solstice, and are about 50 and 40 $msec^{-1}$, respectively. During the Northern fall and spring equinoxes, the maximum mean zonal winds occur at about 65°N and 65°S latitudes and are about 30 $msec^{-1}$. During all seasons except summer the winds are westerly. In the summer seasons of both hemispheres, maximum easterlies of 10 $msec^{-1}$ occur at 10°N and 10°S; secondary maximums of 5 $msec^{-1}$ occur at 70°N and 70°S. At middle latitudes the easterlies are relatively weak and about 2 $msec^{-1}$. The double peak phenomenon in the latitudinal profile was also formed in previous work (Tang, 1966), although the model used was different.

During winter the maximum westerlies occur further south and are stronger then in spring or fall. This is similar to the jet stream migration in the Earth's atmosphere. The wind profiles suggest that a wave regime may be present during the winter and during late spring and early fall. The mean wind at middle latitudes for the equinoctial seasons is about 30 $msec^{-1}$, which is slightly higher (5 $msec^{-1}$) than we obtained previously for a symmetrical regime (Tang, 1966). One expects a higher mean wind at middle latitudes in the wave regime than in the symmeterical regime (Charney, 1959). The computed wind velocity is larger than that of Earth as also found previously in Tang (1966).

In summary, this fairly simple model yields quantitative results on the latitudinal and seasonal variations of mid-atmospheric temperature and zonal wind for Mars. The reliability of the results is open to question because of some of the assumptions inherent in the model and some of the uncertainties in the input data for Mars. The first of these obstacles to reliability can be overcome with the use of an improved general circulation model — such as the numerical model discussed in the next section. The second obstacle to reliability can be overcome as new observational data and analytical studies become available.

2.2 A NUMERICAL MODEL OF THE MARTIAN ATMOSPHERIC GENERAL CIRCULATION

2.2.1 Introduction. As an extension to our previous study of the general circulation of the Martian atmosphere (Tang, 1966) and the recent work presented in the last section, a nonsteady, asymmetrical model is being developed. This model, a combination of the last two models, is a modification of Chen's circulation model which was originally developed for the Earth's atmosphere (Chen, 1965). It includes time variations, eddy transports, and some of the effects of the physical characteristics of the Martian surface (e.g., surface albedo, thermal conductivity, etc.) on the atmospheric circulation. Our main goal is to determine the seasonal variations of the basic zonally averaged motion of the Martian atmosphere and of the underlying surface temperature. The calculations of the surface temperature will be based upon the principle of conservation of energy among radiation, eddy conduction of the atmosphere and thermal conduction of the planetary surface. We shall also examine the influence of large-scale surface thermal conditions on the development of wave disturbances in the hemispheric flow patterns in the nonsteady case.

2.2.2 Basic Model. The fundamental equations are the quasi-geostrophic vorticity equation, the equation of state, the equation of continuity, and the first law of thermodynamics. By a zonally averaging process, we obtain two sets of the above equations. One set consists of the zonally-averaged equations for the mean flow; the other set consists of the finite amplitude perturbation equations for the disturbed flow. Both sets of equations are nonsteady and nonlinear. In the thermodynamic equation we consider not only the radiational processes but also the turbulent heat exchange processes in the atmosphere and heat conduction of the underlying planetary surface. The set of zonal averaged equations for the mean flow and the set of finite amplitude perturbation equations are:

$$\frac{\partial \bar{u}_1}{\partial t} - f_o \bar{v}_1 = - \frac{\partial}{\partial y} (\overline{u_1' v_1'}) + a \frac{\partial^2 \bar{u}_1}{\partial y^2} - k_i (\bar{u}_1 - \bar{u}_3)$$

$$\frac{\partial \bar{u}_3}{\partial t} - f_o \bar{v}_3 = - \frac{\partial}{\partial y} (\overline{u_3' v_3'}) + a \frac{\partial^2 \bar{u}_3}{\partial y^2} - k \left(\frac{3}{2} \bar{u}_3 - \frac{1}{2} \bar{u}_1 \right) + k_i (\bar{u}_1 - \bar{u}_3) \qquad (60)$$

$$f_o \frac{\bar{\omega}_2}{p_2} = \Lambda^2 \left\{ \frac{\partial}{\partial t} (\bar{\psi}_1 - \bar{\psi}_3) + \frac{\partial}{\partial y} [\overline{v_2' (\psi_1' - \psi_3')}] - \frac{R}{f_o c_p} (\bar{Q}_r + \bar{Q}_t) \right\} .$$

$$\nabla^2 \frac{\partial \psi_1'}{\partial t} + \bar{u}_1 \frac{\partial \zeta_1'}{\partial x} + v_1' \left(\frac{\partial \bar{\zeta}_1}{\partial y} + \beta \right) + u_1' \frac{\partial \zeta_1'}{\partial x} + v_1 \frac{\partial \zeta_1'}{\partial y} - f_o \frac{\omega_2'}{p_2} = a\nabla^2 \zeta_1' - k_i (\zeta_1' - \zeta_3')$$

$$\nabla^2 \frac{\partial \psi_3'}{\partial t} + \bar{u}_3 \frac{\partial \zeta_3'}{\partial x} + v_3' \left(\frac{\partial \bar{\zeta}_3}{\partial y} + \beta \right) + u_3' \frac{\partial \zeta_3'}{\partial x} + v_3' \frac{\partial \zeta_3'}{\partial y} + f_o \frac{\omega_2'}{p_2} =$$

$$= a\nabla^2 \zeta_3' - k \left(\frac{3}{2} \zeta_3' - \frac{1}{2} \zeta_1' \right) + f_o \frac{\omega_4'}{p_2} + k_i (\zeta_1' - \zeta_3') \ , \qquad (61)$$

$$f_o \frac{\omega_2'}{p_2} = \Lambda^2 \left[\frac{\partial}{\partial t} (\psi_1' - \psi_3') + \bar{u}_2 \frac{\partial}{\partial x} (\psi_1' - \psi_3') - (\bar{u}_1 - \bar{u}_3) v_2' + u_2' \frac{\partial}{\partial x} (\psi_1' - \psi_3') + \right.$$

$$\left. + v_2' \frac{\partial}{\partial y} (\psi_1' - \psi_3') - \frac{R}{f_o c_p} (Q_r' + Q_t') \right] \ .$$

where $u, v, \omega = \frac{dx}{dt}, \frac{dy}{dt}, \frac{dp}{dt}$,

ζ = the relative vorticity,

$\beta = \frac{df_o}{dy}$,

f_o = the mean Coriolis parameter,

$k_i = \frac{\mu g^2}{\alpha_2 p_2^2}$,

μ = dynamic coefficient of eddy viscosity in the vertical direction,

a = the coefficient of kinematic eddy viscosity in the lateral direction,

$\alpha_2 = \frac{\phi_1 - \phi_3}{p_2}$,

p_2 = pressure at middle of atmosphere,

∇^2 = Laplacian operator,

k = a proportional constant for the frictional stress near surface,

g = acceleration of gravity,

ϕ = geopotential,

t = time,

$$\Lambda^2 = \frac{f_o^2}{RT_2}\left(\frac{\theta_2}{\theta_1 - \theta_3}\right)$$ - a measure of static stability

θ = potential temperature,

$\psi = \phi/f_o$ = geostrophic stream function,

R = gas constant for Martian atmosphere,

c_p = specific heat at constant pressure for Martian atmosphere,

Q_r, Q_t = rate of heating per unit mass due to radiation and turbulence, respectively,

$\overline{(\quad)}$ = zonal averaged quantity

$(\quad)'$ = perturbed quantity,

and the subscripts 0, 1, 2, 3, and 4 represent the pressure levels at p = 0, $\frac{1}{4}\,p_s$, $\frac{1}{2}\,p_s$, $\frac{3}{4}\,p_s$ and p_s, and p_s is the atmospheric pressure at surface of Mars.

The various heat exchange processes are modeled as follows. The radiative heating or cooling of the atmosphere per unit mass consists of three major parts: the absorption of solar radiation; the absorption of surface emitted long wave radiation; and the upward and downward emission of long wave radiation. The solar radiation is a function of time and latitude. Long wave radiation is a function of the surface temperature and the mean temperature of an entire atmospheric column, both of which vary with time, latitude, and longitude. The turbulent heat exchange process includes both horizontal and vertical exchanges. A simple austauch hypothesis is used in this model. The eddy transport of heat from the planetary surface is a function of atmospheric and surface temperature. Since both the radiative and turbulent heat exchange processes between surface and atmosphere depend upon the surface temperature, it is important to include the effects of a nonuniform Martian surface on the surface temperature. For example, the polar caps, bright areas, and dark areas are evidently composed of different materials with different thermal properties. Therefore, in the equation of thermal conduction of the Martian surface, which is used to obtain the surface temperature, the thermal conductivity and diffusivity (Carslaw and Jaeger, 1959) are expressed as functions of Martian longitude and latitude, using Sinton and Strong's (1960) values for dark and bright areas and Geiger's (1965) values for ice. We have written expressions for thermal conductivity and diffusivity as two different truncated Fourier series in horizontal coordinates for the planet Mars, according to the dark and bright area distribution, as

$$\lambda^*(x,y) = \lambda^*_{oo} + \lambda^{*\prime} = \lambda^*_{oo} +$$

$$+ \sum_{m=1}^{6} \left[(\lambda^{*\prime})_{m1} \cos m \frac{2\pi}{L} x + (\lambda^{*\prime})_{m2} \sin m \frac{2\pi}{L} x \right] \cos \frac{\pi}{2W} y +$$

$$+ \sum_{m=1}^{6} \left[(\lambda^{*\prime})_{m3} \cos m \frac{2\pi}{L} x + (\lambda^{*\prime})_{m4} \sin m \frac{2\pi}{L} x \right] \sin \frac{\pi}{W} y + \qquad (62)$$

$$+ \sum_{m=1}^{6} \left[(\lambda^{*\prime})_{m5} \cos m \frac{2\pi}{L} x + (\lambda^{*\prime})_{m6} \sin m \frac{2\pi}{L} x \right] \cos \frac{3\pi}{2W} y,$$

$$b^*(x,y) = b^*_{oo} + b^{*\prime} = b^*_{oo} +$$

$$+ \sum_{m=1}^{6} \left[(b^{*\prime})_{m1} \cos m \frac{2\pi}{L} x + (b^{*\prime})_{m2} \sin m \frac{2\pi}{L} x \right] \cos \frac{\pi}{2W} y +$$

$$+ \sum_{m=1}^{6} \left[(b^{*\prime})_{m3} \cos m \frac{2\pi}{L} x + (b^{*\prime})_{m4} \sin m \frac{2\pi}{L} x \right] \sin \frac{\pi}{W} y + \qquad (63)$$

$$+ \sum_{m=1}^{6} \left[(b^{*\prime})_{m5} \cos m \frac{2\pi}{L} x + (b^{*\prime})_{m6} \sin m \frac{2\pi}{L} x \right] \cos \frac{3\pi}{2W} y.$$

where L = the length of the latitude circle at 45°N or S,

2W = the length of one-half of the meridian (y = W at pole and y = W at equator).

The coefficients of the set of Fourier series for representing these thermal parameters are ready to be determined by solving two 36 x 36 matrices. Similarly, the Fourier series for Martian surface albedo are also ready to be determined. Solutions of these matrices will be obtained with the use of an IBM 7094.

The total heating rate per unit mass of atmosphere at different positions on Mars has been written in an analytical form. Values of the insolation and latitudinal derivative of the insolation as a function of time of year, at six hour intervals, smoothing out diurnal variations, are being obtained.

Since the surface temperature is important for the nonadiabatic heating of the atmosphere, we must solve the heat conduction equation and mean zonal motion equation simultaneously. As a first step in the solution of the problem, we are going to obtain the mean zonal surface temperature and mean zonal motion as a function of time for a period of a Martian year without considering eddy momentum transport.

To keep the model consistent, the solutions of all perturbation (finite amplitude) quantities are expressed in the form of double Fourier series. For example, the perturbed motion may be written as

$$\psi_1'(x,y,t) = \sum_{m=1}^{6} \left[(\psi_1')_{m1} \cos m \frac{2\pi}{L} x + (\psi_1')_{m2} \sin m \frac{2\pi}{L} x \right] \cos \frac{\pi}{2W} y +$$

$$+ \sum_{m=1}^{6} \left[(\psi_1')_{m3} \cos m \frac{2\pi}{L} x + (\psi_1')_{m4} \sin m \frac{2\pi}{L} x \right] \sin \frac{\pi}{W} y + \qquad (64)$$

$$+ \sum_{m=1}^{6} \left[(\psi_1')_{m5} \cos m \frac{2\pi}{L} x + (\psi_1')_{m6} \sin m \frac{2\pi}{L} x \right] \cos \frac{3\pi}{2W} y,$$

where subscripts 1 represents level 1, L is the length of the latitude circle at $45^{\circ}N$, and $(\psi_1')_{m1}$, etc. are the Fourier coefficients which are the functions of the time t. The coefficients of these Fourier series are to be obtained by an electronic computer.

2.2.3 The Working Equations.

2.2.3.1 The Working Equations For the Mean Surface Temperature. The basic finite difference equation for the time differential of the Martian surface temperature can be simply written as

$$b^* \frac{\partial^2}{\partial z^2} T^{*t+\Delta t} = \frac{T^{*t+\Delta t} - T^{*t}}{\Delta t} \qquad (65)$$

where b^* = the temperature-conduction coefficient of the Martian surface

Δt = the time interval used in the computation

T^* = the surface temperature

z = the vertical distance from surface

and the superscripts represent the time as indicated. The quantity T^{*t} is the initial input for each time step and is obtained from the prior step.

The boundary condition at the surface of Mars is the energy balance equation, which simply states that the total energy is a balance among the short and long wave radiations arriving at the surface, the long wave radiation emitted by the Martian surface, and the heat fluxes conducted to the atmosphere through an eddy transport process and to the soil through molecular conduction. The boundary conditions can be written as

$$\left[\lambda^* \frac{\partial T^*}{\partial z} + \frac{\lambda}{H_2} T^* + \sigma T^{*4}\right]^{t+\Delta t} = \left[\frac{\lambda}{H_2} T_2 + S_4 + \sigma T_2^4 - F(T_2)\right]^{t+\Delta t}$$

at $z = 0$,

and (66)

$$T^{*t+\Delta t} = 0$$

at $z = -\infty$

where λ = the eddy heat transfer coefficient of the Martian atmosphere

λ^* = the molecular heat conduction coefficient of the Martian surface

σ = the Stefan-Boltzmann constant

H_2 = the thickness between level 2 and level 4 (level 4 corresponds to the surface level and level 2 is the constant pressure level at which the pressure is one-half of the surface pressure)

T_2 = the temperature at level 2 = $\frac{f_o}{R_o}(\psi_1 - \psi_3)$

(ψ_1, ψ_3) = stream functions at level 1 and 3 respectively (level 1 is the constant pressure level at which the pressure is one-fourth of the surface pressure and level 3 is the constant pressure level at which the pressure is three-fourths of the surface pressure)

T^* = the temperature at level 4

S_4 = the solar radiation reaching the surface of Mars.

$$F(T) = \left[c_1 \exp\left(-\frac{c_2}{\ell T}\right)\left(\frac{T}{c_2 \ell^3} + \frac{3T^2}{c_2^2 \ell^2} + \frac{6T^3}{c_2^3 \ell} + \frac{6T^4}{c_2^4}\right)\right]_{\ell_1}^{\ell_2}$$

$$+ \left[c_1 \exp\left(-\frac{c_2}{\ell T}\right)\left(\frac{T}{c_2 \ell^3} + \frac{3T^2}{c_2^2 \ell^2} + \frac{6T^3}{c_2^3 \ell} + \frac{6T^4}{c_2^4}\right)\right]_{\ell_3}^{\ell_4} \qquad (67)$$

where $\ell_1 = 0$, $\ell_2 = 13\mu$, $\ell_3 = 17\mu$, and $\ell_4 = \infty$; $c_1 = 3.7413 \times 10^{-5}$ erg cm^2 sec^{-1} and $c_2 = 1.4388$ cm deg.

For practical purposes, the flux of long wave radiation from the atmosphere, E, may be assumed as

$$E = \epsilon_a \sigma T^4$$

where ϵ_a is the emissivity of the Martian atmosphere and is approximately equal to 0.16 on the average (House, 1966). If the following relation is valid (Adem, 1962)

$$E = \sigma T^4 - F(T) \qquad (68)$$

then the corresponding F may be written

$$F = (1-\epsilon_a)\, \sigma T^4 = 0.84\, \sigma T^4 \qquad (69)$$

In the actual computation, we shall use this approximation rather than (67).

The final solution for surface temperature, T^*, satisfying the difference equation and the boundary conditions as specified above, is

$$\overline{T}^{*t+\Delta t}\Big|_{z=0} = \frac{\bar{L}}{\dfrac{\lambda^*_{oo}}{\sqrt{b^*_{oo}\Delta t}} + \left(\dfrac{\lambda}{H_2} + 4\sigma\bar{\bar{T}}^{*3}\right)} + \frac{\dfrac{\lambda^*_{oo}}{\sqrt{b^*_{oo}\Delta t}}\,\overline{T}^{*t}}{\dfrac{\lambda^*_{oo}}{\sqrt{b_{oo}\Delta t}} + \left(\dfrac{\lambda}{H_2} + 4\,\bar{\bar{T}}^{*3}\right)} \qquad (70)$$

where

$$\bar{L} = \left[\left(\frac{\lambda}{H_2} - \frac{F(\bar{T})}{\bar{T}_2} + 4\sigma\bar{\bar{T}}_2^3\right)\frac{f_o}{R}\,(\bar{\psi}_1 - \bar{\psi}_3) + \bar{S}_4\right]^{t+\Delta t} \tag{71}$$

$(\lambda^*_{oo}, b^*_{oo})$ = the mean values of the heat conduction and temperature-conduction coefficients of the surface respectively,

and the bars over T, L, ψ, and S represent the mean zonal values.

Since L is a function of ψ_1 and ψ_3, we must solve for T^* simultaneously with the mean zonal motion by a finite time interval step-by-step process for about 1-1/2 Martian years. Based upon previous experience, a time interval of 6 hours would be appropriate for the grid size adopted in this model; an integration will need about 4000 time steps.

2.2.3.2 The Working Equations For Mean Zonal Wind Velocities. The basic zonal wind velocities for different meridional grid points at levels 1 and 3 can be obtained by solving the following six simultaneous equations. These equations will be used as working equations in the numerical computations. They are listed below.

$$\frac{\partial}{\partial t}\bar{u}_{1+1} + \frac{\partial}{\partial t}\bar{u}_{3+1} = R_1\,\bar{u}_{1+1} + R_2\,\bar{u}_{1+0} + 0 + R_3\,\bar{u}_{3+1} + R_2\,\bar{u}_{3+0} - \frac{\partial}{\partial y}\left(\overline{u_1' v'} + \overline{u_3' v_3'}\right)_{+1}, \tag{72}$$

$$\frac{\partial}{\partial t}\bar{u}_{1+0} + \frac{\partial}{\partial t}\bar{u}_{3+0} = R_2\,\bar{u}_{1+1} + R_1\,\bar{u}_{1+0} + R_2\,\bar{u}_{1-1} + R_2\,\bar{u}_{3+1} + R_3\,\bar{u}_{3+0} + R_2\,\bar{u}_{3-1} - \frac{\partial}{\partial y}\left(\overline{u_1' v'} + \overline{u_3' v_3'}\right)_{+0}, \tag{73}$$

$$\frac{\partial}{\partial t}\bar{u}_{1-1} + \frac{\partial}{\partial t}\bar{u}_{3-1} = R_2\,\bar{u}_{1+0} + R_1\,\bar{u}_{1-1} + R_2\,\bar{u}_{3+0} + R_3\,\bar{u}_{3-1} - \frac{\partial}{\partial y}\left(\overline{u_1' v_1'} + \overline{u_3' v_3'}\right)_{-1}, \tag{74}$$

$$- R_o \frac{\partial}{\partial t} \bar{u}_{1+1} + \frac{\partial}{\partial t} \bar{u}_{1+0} + R_o \frac{\partial}{\partial t} \bar{u}_{3+1} - \frac{\partial}{\partial t} \bar{u}_{3+0} = R_4 \bar{u}_{1+1} + R_5 \bar{u}_{1+0} + R_7 \bar{u}_{3+1}$$

$$+ R_8 \bar{u}_{3+0} - R_2 \bar{u}_{3-1} - \frac{W^2}{4} \frac{\partial^3}{\partial y^3} (\overline{u' v_1'} - \overline{u_3' v_3'})_{+1}$$

$$- 2\Lambda^2 \frac{\partial^2}{\partial y^2} [\overline{v_2'(\psi_1' - \psi_3')}]_{+1} - R_{10} \left\{ \frac{\partial}{\partial y} [(1 - \bar{\Gamma}) \bar{S}_o] \right.$$

$$\left. - \frac{\partial F(T^*)}{\partial y}\bigg|_{z=0} - \lambda^*_{oo} \frac{\partial}{\partial y} \left(\frac{\partial T^*}{\partial z} \right)_{z=0} \right\}_{+1} , \qquad (75)$$

$$\frac{\partial}{\partial t} \bar{u}_{1+1} - R_o \frac{\partial}{\partial t} \bar{u}_{1+0} + \frac{\partial}{\partial t} \bar{u}_{1-1} - \frac{\partial}{\partial t} \bar{u}_{3+1} + R_o \frac{\partial}{\partial t} \bar{u}_{3+0} - \frac{\partial}{\partial t} \bar{u}_{3-1}$$

$$= R_5 \bar{u}_{1+1} + R_6 \bar{u}_{1+0} + R_5 \bar{u}_{1-1} + R_8 \bar{u}_{3+1} + R_9 \bar{u}_{3+0} + R_8 \bar{u}_{3-1}$$

$$- \frac{W^2}{4} \frac{\partial^3}{\partial y^3} (\overline{u_1' v_1'} - \overline{u_3' v_3'})_{+0} - \frac{W^2}{4} 2\Lambda^2 \frac{\partial^2}{\partial y^2} [\overline{v_2'(\psi_1' - \psi_3')}]_{+0}$$

$$- R_{10} \left\{ \frac{\partial}{\partial y} [(1 - \bar{\Gamma}) \bar{S}_o] - \frac{\partial F(T^*)}{\partial y}\bigg|_{z=0} - \lambda^*_{oo} \frac{\partial}{\partial y} \left(\frac{\partial \bar{T}^*}{\partial z} \right)_{z=0} \right\}_{+0} , \qquad (76)$$

$$\frac{\partial}{\partial t} \bar{u}_{1+0} - R_o \frac{\partial}{\partial t} \bar{u}_{1-1} - \frac{\partial}{\partial t} \bar{u}_{3+0} + R_o \frac{\partial}{\partial t} \bar{u}_{3-1} = R_2 \bar{u}_{1+1} + R_5 \bar{u}_{1+0} + R_4 \bar{u}_{1-1}$$

$$- R_2 \bar{u}_{3+1} + R_8 \bar{u}_{3+0} + R_7 \bar{u}_{3-1} - \frac{W^2}{4} \frac{\partial^3}{\partial y^3} (\overline{u_1' v_1'} - \overline{u_3' v_3'})_{-1}$$

$$- \frac{W^2}{4} 2\Lambda^2 \frac{\partial^2}{\partial y^2} [\overline{v_2'(\psi_1' - \psi_3')}]_{-1} - R_{10} \left\{ \frac{\partial}{\partial y} [(1 - \bar{\Gamma}) \bar{S}_o] \right.$$

$$\left. - \frac{\partial F(T^*)}{\partial y}\bigg|_{z=0} - \lambda^*_{oo} \frac{\partial}{\partial y} \left(\frac{\partial \bar{T}^*}{\partial z} \right)_{z=0} \right\}_{-1} , \qquad (77)$$

where $R_0 = 2\left(1 + \frac{1}{4}\Lambda^2 W^2\right)$,

$$R_1 = \frac{k}{2} - 8\frac{a}{W},$$

$$R_2 = \frac{4a}{W^2},$$

$$R_3 = -\frac{3}{2}k - 8\frac{a}{W^2},$$

$$R_4 = 20\frac{a}{W^2} + k + 4a\Lambda^2 - \frac{W^2}{4}\frac{\Lambda^2}{c_p}\frac{g}{2p_2}\frac{\partial}{\partial y}\left[\sigma\bar{\bar{T}}_2^4 - F(\bar{\bar{T}}_2)\right]\frac{1}{\frac{\partial \bar{\bar{T}}_2}{\partial y}} + 4k_i,$$

$$R_5 = 16\frac{a}{W^2} - \frac{k}{2} - 2a\Lambda^2 - 2k_i,$$

$$R_6 = 24\frac{a}{W^2} + k + 4a\Lambda^2 + \frac{W^2}{4}\frac{\Lambda^2}{c_p}\frac{g}{2p_2}\frac{\partial}{\partial y}\left[\sigma\bar{\bar{T}}_2^4 - F(\bar{\bar{T}}_2)\right]\frac{1}{\frac{\partial \bar{\bar{T}}_2}{\partial y}} + 4k_i,$$

$$R_7 = -20\frac{a}{W^2} - 3k - 4a\Lambda^2 - \frac{W^2}{4}\frac{\Lambda^2}{c_p}\frac{g}{2p_2}\frac{\partial}{\partial y}\left[\sigma\bar{\bar{T}}_2^4 - F(\bar{\bar{T}}_2)\right]\frac{1}{\frac{\partial \bar{\bar{T}}_2}{\partial y}} - 4k_i,$$

$$R_8 = 16\frac{a}{W^2} + \frac{3}{2}k + 2a\Lambda^2 + 2k_i,$$

$$R_9 = -24\frac{a}{W^2} - 3k - 4a\Lambda^2 - \frac{W^2}{4}\frac{\Lambda^2}{c_p}\frac{g}{2p_2}\frac{\partial}{\partial y}\left[\sigma\bar{\bar{T}}_2^4 - F(\bar{\bar{T}}_2)\right]\frac{1}{\frac{\partial \bar{\bar{T}}_2}{\partial y}} - 4k_i,$$

$$R_{10} = \frac{W^2}{4}\frac{\Lambda^2}{c_p}\frac{Rg}{f_o p_2},$$

u_{1-2}, u_{1-1}, u_{1+0}, u_{1+1}, and u_{1+2} = quantity u at level 1 on the points y = W, $-\frac{1}{2}$W, 0, $\frac{1}{2}$W, and w respectively

a = radius of Mars,

W = one half of the distance between pole and equator,

c_p = specific heat of Martian atmosphere at constant pressure,

f_o = Coriolis parameter,

p_2 = atmospheric pressure at level 2,

g = gravitational acceleration,

R = gas constant

k = a proportional constant for frictional stress in vertical direction,

k_i = internal friction,

$$\Lambda^2 = \frac{f_o^2}{RT_2} \times \frac{\theta_2}{\theta_1 - \theta_3} ,$$

$\theta_1, \theta_2, \theta_3$ = potential temperature at levels 1, 2, and 3, respectively.

2.2.3.3 The Working Equation For the Finite Amplitude Perturbed Motion. Substituting the perturbation of heating per unit mass into Equation (62), eliminating ω_2, using the Fourier series and keeping all the nonlinear terms yeilds the following working equations of atmospheric disturbance.

$$M_1 \frac{\partial}{\partial t}(\psi_1')_{mn} + \Lambda^2 \frac{\partial}{\partial t}(\psi_3')_{mn} = - M_2(\psi_1')_{mn} + M_3(\psi_1')_{mn+1} - M_4(\psi_3')_{mn} +$$

$$+ M_5(\psi_3')_{mn+1} + M_{11}(T^{*\prime}_{z=0})_{mn} + M_6\lambda^*_{oo}\left(\frac{\partial T^{*\prime}}{\partial Z}\bigg|_{z=0}\right) + N_{mn} , \qquad (78)$$

$$M_1 \frac{\partial}{\partial t}(\psi_1')_{mn+1} + \Lambda^2 \frac{\partial}{\partial t}(\psi_3')_{mn+1} = - M_3(\psi_1')_{mn} - M_2(\psi_1')_{mn+1} - M_5(\psi_3')_{mn} -$$

$$- M_4(\psi_3')_{mn+1} + M_{11}(T^*_{z=0})_{mn+1} + M_6\lambda^*_{oo}\left(\frac{\partial T^{*\prime}}{\partial Z}\bigg|_{z=0}\right)_{mn+1} + N_{mn+1}, \qquad (79)$$

$$\Lambda^2 \frac{\partial}{\partial t}(\psi_1')_{mn} + M_1 \frac{\partial}{\partial t}(\psi_3')_{mn} = - M_7(\psi_1')_{mn} + M_8(\psi_1')_{mn+1} - M_9(\psi_3')_{mn} +$$

$$+ M_{10}(\psi_3')_{mn+1} - M_{11}(T^{*\prime}_{z=0})_{mn} - M_6\lambda^*_{oo}\left(\frac{\partial T^{*\prime}}{\partial Z}\bigg|_{z=0}\right)_{mn} + \tilde{N}_{mn} \qquad (80)$$

$$\Lambda^2 \frac{\partial}{\partial t} (\psi_1')_{mn+1} + M_1 \frac{\partial}{\partial t} (\psi_3')_{mn+1} = - M_8(\psi_1')_{mn} - M_7(\psi_1')_{mn+1} -$$

$$- M_{10}(\psi_3')_{mn} - M_9(\psi_3')_{mn+1} - M_{11}(T^{*\prime}_{z=0})_{mn+1} - M_6\lambda^*_{oo} \left(\frac{\partial T^{*\prime}}{\partial Z}\bigg|_{z=0} \right)_{mn+1} + \tilde{N}_{mn+1} \tag{81}$$

$$(m = 1,2,\ldots,6, \quad n = 1,3,5)$$

where

$$M_1 = - \left[(m^2 + 2j^2) \frac{4\pi^2}{L^2} + \Lambda^2 \right],$$

$$M_2 = (m^2 + 2j^2) \frac{4\pi^2}{L^2} (a M_1 - k_i) - 4 \left[4\sigma \bar{\bar{T}}_2^3 \; T_2' - F (\bar{\bar{T}}_2 + \bar{T}_2 + T_2') + \right.$$

$$\left. + F (\bar{\bar{T}}_2 + \bar{T}_2) \right] \frac{g\Lambda^2}{2p_2 c_p} \frac{1}{T_2'}$$

$$M_3 = m \frac{2\pi}{L} \left[- M_1 \bar{u}_{1+0} - \beta + \frac{4}{W^2} (\bar{u}_{1+1} - 2\bar{u}_{1+0} + \bar{u}_{i-1}) - \Lambda^2 (\bar{u}_{1+0} - \bar{u}_{3+0}) \right],$$

$$M_4 = (m^2 + 2j^2) \frac{4\pi^2}{L^2} (a\Lambda^2 + k_i) + 4 \left[4\sigma \bar{\bar{T}}_2^3 \; T_2' - F (\bar{\bar{T}}_2 + \bar{T}_2 + T_2') + \right.$$

$$\left. + F (\bar{\bar{T}}_2 + \bar{T}_2) \right] \frac{g\Lambda^2}{2p_2 c_p} \frac{1}{T_2'}$$

$$M_5 = m \frac{2\pi\Lambda^2 u_{1+0}}{L}$$

$$M_6 = \frac{\Lambda^2 Rg}{2p_2 f_0 c_p}$$

$$M_7 = M_4 + (m^2 + 2j^2) \frac{4\pi^2}{L^2} \cdot \left(\frac{k}{2} + k_i \right)$$

$$M_8 = - m \frac{2\pi\Lambda^2 u_{3+0}}{L},$$

$$M_9 = M_2 - (m^2 + 2j^2) \frac{4\pi^2}{L^2} \cdot \left(\frac{3k}{2} + k_i \right)$$

$$M_{10} = m \frac{2\pi}{L} \left[- M_1 \bar{u}_{3+0} - \beta + \frac{4}{W^2} (\bar{u}_{3+1} - 2\bar{u}_{3+0} + \bar{u}_{3-1}) + \Lambda^2 (\bar{u}_{1+0} - \bar{u}_{3+0}) \right],$$

$$M_{11} = \frac{g\Lambda^2 R}{f_o p_2 c_p} \left[- F (\bar{\bar{T}}_4 + \bar{T}_4 + T'_4) + F (\bar{\bar{T}} + \bar{T}_4) \right] \frac{1}{T'_4}$$

j=1 when n=1, j=2 when n=3, and j=3 when n=5. N_{mn} are the terms derived from the quadratic terms of the vorticity advection and the temperature advection at level 1 and $\tilde{N}_{mn}$ are the terms derived from the quadratic terms of the vorticity advection and the temperature advection at level 3.

It is planned to integrate these equations numerically using the Runge-Kutta method. As a first approximation, we assume that the non-linear terms in Equations (72) to (77) can be neglected. Then these six equations for the mean zonal winds will be solved simulataneously with the solution for the mean surface temperature.

During the next year, the equations for the mean zonal velocities and the mean zonal temperatures will be programmed. Once the mean zonal velocities and temperatures are obtained, they can be used as input to the perturbation equations, solutions of which will provide information on the longitudinal variations of the circulation and temperature field. The perturbation equations for this problem will be also completed during the next year.

REFERENCES

Adem, J., 1962: On the theory of the general circulation of the atmosphere. Tellus, 14, 102-105.

Belton, M. J., and D. M. Hunten, 1966: The abundance and temperature of CO_2 in the Martian atmosphere. Ap. J., 145, 454-467.

Burch, D. E., D. Gryvnak, and D. Williams, 1960: Infrared absorption by carbon dioxide, Report, Ohio State University.

Carslaw, H. S., and J. C. Jaeger, 1959: Conduction of Heat in Solids. Oxford University Press, London, 510 pp.

Charney, J., 1959: On the general circulation of the atmosphere. The Atmosphere and the Sea in Motion. The Rockefeller Institute Press, New York, 509 pp.

Chen, Y-S, 1965: A numerical experiment on the atmospheric circulation based on the two-level quasi-geostrophic model. Scientia Sinica, 14, 246-266.

Curtis, A., and R. Goody, 1956: Thermal radiation in the upper atmosphere. Proc. Roy. Soc. (A), 236, 193-206.

Dent, W. A., M. J. Klein, and H. D. Aller, 1965: Measurements of Mars at λ 3.75 cm from February to June 1965. Ap. J., 142, 1685-1688.

de Vaucouleurs, G., 1964: Geometric and photometric parameters of the terrestrial planets. Icarus, 3, 187-235.

Fjeldbo, G., W. Fjeldbo, and V. Eshleman, 1966: Models for the atmosphere of Mars based upon the Mariner 4 occultation experiment. J. Geophys. Res., 71, 2307-2316.

Geiger, R., 1965: The Climate near the Ground. Harvard University Press, Cambridge, Mass., 611 pp.

Goody, R., 1957: The atmosphere of Mars. Weather, 12, 3.

Hess, S. L., and H. L. Panofsky, 1951: Compendium of Meteorology. Amer. Meteor. Soc., Boston, Mass., 1334 pp.

Houghton, J. T., 1963: The absorption of solar infrared radiation by the lower stratosphere. Quart. J. Roy. Met. Soc., 89, 319-331.

House, F., 1966: The seasonal climatology of Mars. In Contributions to Planetary Meteorology. GCA Tech. Rpt. No. 66-8-N, Final Report under Contract NASW-1227.

Howard, J.N., D. L. Burch, and D. Williams, 1955: Near infrared transmission through synthetic atmospheres. G.R.P. 40 (astia AD-87679).

Hughes, M. P., 1966: Planetary observations at a wavelength of 6 cm. Planetary and Space Sci., 14, 1017-1022.

Kaplan, L., G. Münch, and H.Spinrad, 1964: An analysis of the spectrum of Mars. Ap. J., 139, 1-15.

Kellerman, K. I., 1966: The thermal radio emission from Mercury, Venus, Mars, Saturn, and Uranus. Icarus, 5, 478-490.

Kliore, A., D. Cain, G. Levy, V. Eshleman, G. Fjeldbo, and F. Drake, 1965: Occultation experiment: Results of the first direct measurements of Mars atmosphere and ionosphere. Science, 149, 1243-1248.

Kliore, A., D. Cain, G. Levy, V. Eshleman, G. Fjeldbo, and F. Drake, 1966: Preliminary results of the Mariner IV occultation measurements of the atmosphere of Mars. In: Proceedings of the Caltech-JPL Lunar and Planetary Conference, Sept. 13-18, 1965, 257-266.

Kliore, A., D. Cain, and G. Levy, 1966: Radio occultation measurements of the Martian atmosphere over two regions by the Mariner IV space probe. COSPAR, Internat. Space Science Symp., 7th, Vienna, May 10-19, 1966.

Leighton, R.B., and B.C. Murray, 1966: Behavior of carbon dioxide and other volatiles on Mars. Science, 153, 136-144.

Leovy, C.B., 1966: Radiative-convective equilibrium calculations for a two-layer Mars atmosphere. Rand Memo. RM-5017, 41 pp.

Manabe, S., and R.F. Strickler, 1964: Thermal equilibrium of the atmosphere with convective adjustment. J. Atmos. Sci., 21, 361-385.

Mintz, Y., 1961: The general circulation of planetary atmospheres. The Atmospheres of Mars and Venus. Pub. 944, NAS-NRO, Wash., D.C.

Ohring, G., and J. Mariano, 1966: The vertical temperature distribution in the Martian atmosphere. J. Atmos. Sci., 23, 251-255.

Owen, T., 1966: The composition and surface pressure of the Martian atmosphere: Results from the 1965 opposition. Ap. J., 146, 257-270.

Prabhakara, C., and J. S. Hogan, Jr., 1965: Ozone and carbon dioxide heating in the Martian atmosphere. J. Atmos. Sci., 22, 97-109.

Rodgers, C.D., and C.D. Walshaw, 1966: The computation of infrared cooling rates in planetary atmospheres. Quart. J. Roy. Met. Soc., 92, 67-92.

Seeley, J. S., and J. T. Houghton, 1961: Spectroscopic observations of the vertical distribution of some minor constituents of the atmosphere. Infrared Phys., 1, 116-132.

Sinton, W. M., and J. Strong, 1960: Radiometric observations of Mars. Ap. J., 131, 459-469.

Smagorinsky, J., S. Manabe, and J. L. Halloway, Jr., 1965: Numerical results from a nine-level general circulation model of the atmosphere. Mon. Wea. Rev., 93, 727-768.

Spinrad, H., R. A. Schorn, R. Moore, L. P. Giver, 1966: High dispersion spectroscopic observations of Mars. I. The CO_2 content and surface pressure. Ap. J., 146, 331-338.

Tang, W., 1966: A study of the general circulation of the Martian atmosphere based upon the result of the occultation experiment from Mariner IV. Proc. of the 9th COSPAR meeting, Vienna, Austria, 1966. (In print).

APPENDIX

APPENDIX

ACCURACY OF LORENTZ LINE SHAPE

At high altitudes (low pressures) the shape of absorption lines changes from a Lorentz shape, which is assumed in our calculations of Martian temperatures, through a mixed shape to the Doppler shape. The height in the Martian atmosphere at which the transition to a Doppler shape takes place can be estimated following Rodgers and Walshaw (1966). A mixed line consists of a Doppler core and Lorentz wings. If the line is fully absorbed as far out as the Lorentz wings, the Doppler core makes no contribution to the transmission gradient. The point at which the Lorentz wings begin is given by

$$k_{\nu_L} = k_{\nu_D} \tag{A-1}$$

where $k_{\nu L}$ is the Lorentz absorption coefficient and $k_{\nu D}$ is the Doppler absorption coefficient. Substituting the complete expressions for these absorption coefficients, we obtain

$$\frac{k}{\pi} \frac{\alpha_L}{\nu^2 + \alpha_L^2} = \frac{k}{\alpha_D \sqrt{\pi}} \exp\left(-\frac{\nu^2}{\alpha_D^2}\right) \tag{A-2}$$

where k is the line intensity, ν is measured from the line center, and α_L and α_D are the Lorentz and Doppler half-widths. With $x = \nu/\alpha_D$ and $y = \alpha_L/\alpha_D$, (A-2) becomes

$$y = \sqrt{\pi}\ (x^2 + y^2)\ e^{-x^2} \ . \tag{A-3}$$

If the criterion of blackness is taken to be about 2 percent transmission, then a Lorentz line is "black" out to that frequency at which the transmission is 0.02, or

$$T = \exp(-k_\nu m) = \exp - \left[\frac{k\alpha_L m}{\pi(\nu^2 + \alpha_L^2)} \right] = 0.02 \ . \tag{A-4}$$

This corresponds to a value of x given by

$$x = y \left[\frac{km}{4\pi\alpha_L} - 1 \right]^{1/2} \ . \tag{A-5}$$

The amount of absorber, m, between a pressure level p and the top of the atmosphere, and the average Lorentz half-width, α_L, for such a path are given by

$$m = \frac{wp}{g} \qquad \text{and} \qquad \alpha_L = \frac{\alpha_{L_s} p}{2p_s} \tag{A-6}$$

where α_{L_s} is the Lorentz half-width at STP. Substituting these values into (A-5), we obtain

$$x = y \left[\frac{kwp_s}{2g\pi\alpha_{L_s}} - 1 \right]^{1/2} . \tag{A-7}$$

Letting $\eta = kwp_s/2\pi\alpha_{L_s} g$, and combining (A-7) with (A-3), we obtain

$$y\eta\sqrt{\pi} \exp\left[- y^2(\eta - 1) \right] = 1 . \tag{A-8}$$

This relationship determines the height above which Doppler broadening must be considered. According to Rodgers and Walshaw (1966), the value of η for the 15μ CO_2 band in the Earth's atmosphere is 1200. For a Martian CO_2 mass mixing ratio of 0.5 and gravitational acceleration of 373 cm sec^{-2}, the value of η in the Martian atmosphere is 2.9×10^3 as large, or 3.5×10^6. From (A-8), we then obtain a value of y equal to 1.62×10^{-3} for Mars' atmosphere. Since

$$y = \frac{\alpha_L}{\alpha_D} = 1.62 \times 10^{-3} ,$$

and $\alpha_D = 7 \times 10^{-4}$ (Rodgers and Walshaw, 1966), then $\alpha_L = 1.13 \times 10^{-6}$. The pressure level in the Martian atmosphere corresponding to this value of α_L is given by

$$p = \frac{\alpha_L}{\alpha_{L_s}} p_s$$

and is equal to 1.6×10^{-2} mb. Thus, below (in height) pressure levels of 1.6×10^{-2} mb, the neglect of Doppler broadening is justified. For a Martian atmosphere scale height of 9 km and surface pressure of 10 mb, this corresponds to a height of 58 km.